

GAMMA-RAY BURST JET BREAKS REVISITED

Xiang-Gao Wang^{1,2,3}, Bing Zhang², En-Wei Liang^{1,3}, Rui-Jing Lu^{1,3}, Jing Li^{1,3}, Long Li^{1,3}

ABSTRACT

Gamma-ray Burst (GRB) collimation has been inferred with the observations of achromatic steepening in GRB light curves, known as jet breaks. Identifying a jet break from a GRB afterglow lightcurve allows a measurement of the jet opening angle and true energetics of GRBs. In this paper, we reinvestigate this problem using a large sample of GRBs that have an optical jet break which is consistent with being achromatic in the X-ray band. Our sample includes 99 GRBs from February 1997 to March 2015 that have optical and, for *Swift* GRBs, X-ray lightcurves that are consistent with the jet break interpretation. Out of 99 GRBs we have studied, 55 GRBs are found to have temporal and spectral behaviors both before and after the break consistent with the theoretical predictions of the jet break models, respectively. These include 53 long/soft (Type II) and 2 short/hard (Type I) GRBs. Only 1 GRB is classified as the candidate of a jet break with energy injection. Another 41 and 3 GRBs are classified as the candidates with the lower and upper limits of the jet break time, respectively. Most jet breaks occur at **90 ks**, with a typical opening angle $\theta_j = (2.5 \pm 1.0)^\circ$. This gives a typical beaming correction factor $f_b^{-1} \sim 1000$ for Type II GRBs, suggesting an even higher total GRB event rate density in the universe. Both isotropic and jet-corrected energies have a wide span in their distributions: $\log(E_{\gamma,\text{iso}}/\text{erg}) = 53.11$ with $\sigma = 0.84$; $\log(E_{\text{K},\text{iso}}/\text{erg}) = 54.82$ with $\sigma = 0.56$; $\log(E_\gamma/\text{erg}) = 49.54$ with $\sigma = 1.29$; and $\log(E_{\text{K}}/\text{erg}) = 51.33$ with $\sigma = 0.58$. We also investigate several empirical correlations (Amati, Frail, Ghirlanda and Liang-Zhang) previously discussed in the literature. We find that in general most of these relations are less tight than before. The existence of early jet breaks and hence small opening angle jets, which were detected in the *Swift* era, is most likely the source of scatter. If one limits the sample to jet breaks later

¹GXU-NAOC Center for Astrophysics and Space Sciences, Department of Physics, Guangxi University, Nanning 530004, China; wangxg@gxu.edu.cn; lew@gxu.edu.cn

²Department of Physics and Astronomy, University of Nevada Las Vegas, NV 89154, USA; zhang@physics.unlv.edu

³Guangxi Key Laboratory for the Relativistic Astrophysics, Nanning 530004, China

than 10^4 s, the Liang-Zhang relation remains tight and the Ghirlanda relation still exists. These relations are derived from Type II GRBs, and Type I GRBs usually deviate from them.

Subject headings: radiation mechanisms: non-thermal — gamma-rays: bursts — method: statistics

1. Introduction

Gamma ray bursts (GRBs) are the most luminous phenomena observed in the universe, with an isotropic γ -ray energy up to $E_{\gamma,\text{iso}} \sim 10^{55}$ erg (Kumar & Zhang 2015). They signify the birth of a stellar-mass black hole or a rapidly rotating magnetized neutron star during the core collapse of massive stars (Type II GRBs) or mergers of compact objects (Type I GRBs) (e.g., Woosley 1993; Paczyński 1998; Woosley & Bloom 2006; Gehrels et al. 2005; Berger 2014; Zhang 2006; Zhang et al. 2007, 2009). Phenomenologically, GRBs are classified based on the burst durations (Kouveliotou et al. 1993), with long GRBs (LGRBs, $T_{90} > 2$ s) mostly correspond to Type II and short GRBs (SGRBs, $T_{90} < 2$ s) mostly correspond to Type I. An important result from the pre-Swift era observations is that Type II GRBs are highly collimated with a typical opening angle of $\sim 5^\circ$ (e.g. Frail et al. 2001; Bloom et al. 2003; Berger et al. 2003). Some empirical correlations, several involving jet opening angles, have been discussed in the literature (e.g. Frail et al. 2001; Amati et al. 2002; Ghirlanda et al. 2004; Liang & Zhang 2005; Wang et al. 2011).

Theoretically, GRB afterglow is essentially independent of the progenitor and central engine, and invokes the interaction between the fireball that produced the GRB and an circumburst medium (CBM) with a density profile generally described as $n(r) \propto r^{-k}$. A generic synchrotron external shock model has been well established to interpret the broad-band afterglow data (e.g., Mészáros & Rees 1997; Sari et al. 1998; Chevalier & Li 2000; Gao et al. 2013). Our recent study (Wang et al. 2015) suggests that the simplest external forward shock models can account for the multi-wavelength afterglow data of at least half of the GRBs. When more advanced modeling (e.g., long-lasting reverse shock, structured jets) is invoked, up to 90% of the afterglows may be interpreted within the framework of the external shock models.

An achromatic, steepening temporal break observed in some afterglow lightcurves suggests that the GRB outflows are collimated. In the fireball external shock model, the burst ejecta moves with a relativistic speed and is assumed to form a conical jet with half opening angle θ_j . As the burst ejecta are decelerated by the ambient, the relativistic beaming angle

$1/\Gamma$ continues to increase with time. When $1/\Gamma > \theta_j$ is satisfied, a steepening break in the afterglow lightcurve (known as the jet break) is predicted. This is mostly due to an edge effect, which is purely geometric: the $1/\Gamma$ cone is no longer filled with emission beyond the jet break time (when $1/\Gamma > \theta_j$). This gives a reduction of flux by $\theta_j^2/(1/\Gamma)^2 = \Gamma^2\theta_j^2$. It has been suggested that a maximized sideways expansion effect may further steepen the light curve (Rhoads 1999; Sari et al. 1999). This theory suggests that sound waves in the jet would cross the jet in the transverse direction when $1/\Gamma > \theta_j$. The cross section of the jet would increase with time, leading to an exponential deceleration of the jet. Later numerical simulations suggested that the sideways expansion effect is not significant, but the post-jet-break decay index could be similar to that predicted in the sideways expansion models (e.g., Zhang & MacFadyen 2009; Granot & Piran 2012).

Extensive studies on the jet break phenomenon have been carried out. In the pre-*Swift* era, several cases of jet break have been observed in the optical band at several days after the GRB trigger (e.g., Rhoads 1999; Sari et al. 1999; Huang et al. 2000; Halpern et al. 2000; Frail et al. 2001; Bloom et al. 2001; Jaunsen et al. 2001; Wei & Lu 2002; Wu et al. 2004; Gao & Wei 2005; Panaiteescu 2005a; Starling et al. 2005; Yonetoku et al. 2005; Zeh et al. 2006; Gorosabel et al. 2006; Liang et al. 2008). However, the achromatic behavior of the break, a prediction of the jet model, could not be confirmed with the optical data only. A rich database of broadband afterglow lightcurves are accumulating after the *Swift* satellite was launched. Many investigations to search for and to study the statistical properties of jet breaks have been carried out based on the XRT data (e.g., Burrows et al. 2006; Grupe et al. 2006; Wang & Mészáros 2006; Burrows & Racusin 2006; Dai et al. 2007; Jin et al. 2007; Nava et al. 2007; Panaiteescu 2007; Willingale et al. 2007; Liang et al. 2008; Kocevski & Butler 2008; de Pasquale et al. 2009; Evans et al. 2009; Kamble et al. 2009; Racusin et al. 2009; Urata et al. 2009; Gao & Dai 2010; Tanvir et al. 2010; Zheng & Deng 2010; Nicuesa Guelbenzu et al. 2011a; Fong et al. 2012, 2014), the optical data (e.g., Dai et al. 2007, 2008; Panaiteescu 2007; Krühler et al. 2009b; Tanvir et al. 2010; Afonso et al. 2011; Filgas et al. 2011; Nicuesa Guelbenzu et al. 2011a; Fong et al. 2014), and the radio data (e.g., Sheth et al. 2003; van der Horst et al. 2005; Fong et al. 2014). The X-ray lightcurves of some GRBs did not show a clear jet break at very late times (Grupe et al. 2006, 2007). Some argued that a jet break may be hidden in the low signal-to-noise ratio (S/N) lightcurves (e.g., Shao & Dai 2007; Sato et al. 2007; Curran et al. 2008). More late time optical observations are needed to reveal late jet breaks and to constrain GRB collimation and energetics (Zhang 2011). Indeed, X-ray observations with *Chandra* X-Ray Telescope have led to detections of some late jet breaks, which allowed a study of the off-axis effect of GRB jets (Zhang et al. 2015). Among the GRBs with optical afterglow detections, only 1/3 were also detected in the radio band. However, there is a lack of GRBs with high quality lightcurves in the radio band to conduct jet break searches.

Based on a rich database of broad-band afterglow up to 2015, this paper aims at a systematic analysis of the jet break features in GRBs. The sample selection and data analysis are described in §2. We use the *closure relations* of the external forward shock model to select the jet break candidates, and the results are presented in §3. A statistical analysis of energetics and luminosity correlations of the jet break sample is presented in §4. Our results are summarized in §5 with some discussion.

We characterize the dependence of the afterglow flux on time and frequency as $F(t, \nu) \propto t^{-\alpha} \nu^{-\beta}$, where α is the temporal decay index, and β is the spectral index. We use the Λ CDM model with cosmological parameters of $\Lambda_M = 0.27$, $\Omega_\Lambda = 0.27$, and $H_0 = 71 \text{ km s}^{-1} \text{ Mpc}^{-1}$ to calculate the energetics of the GRBs.

2. Data Sample

To systematically investigate jet breaks, we collect all the optical afterglow data from the first GRB optical afterglow detected from February 1997 to March 2015. This includes 17 pre-*Swift* GRBs from Liang et al. (2008) that have been studied extensively. A sample of ~ 260 optical lightcurves are compiled from the published papers (e.g. Kann et al. 2010a, 2011) or GCN Circulars after the *Swift* launch. The UVOT data are not included in our sample. For the *Swift* data, we obtain a sample of 85 well-observed GRBs with light curves in both X-ray and optical bands and the constrained spectral indices. Out of these 85 bursts, 82 GRBs have been graded as the achromatic sample consistent with the external shock model (i.e. Gold and Silver samples defined in Wang et al. 2015). We thus select 82 GRBs from the achromatic sample for the purpose of this work. As a result, altogether 99 GRBs are included in our final sample.

Most observations were carried out in the R-band. For those observations carried out in other bands, we correct them to the R band with the optical spectral indices (β_O , with the convention $F_\nu \propto \nu^{-\beta_O}$) collected from the literature assuming that there is no spectral evolution. The correction due to Galactic extinction is taken into account using the reddening map presented by Schlegel et al. (1998). Because of large uncertainties, we do not make corrections to the extinction in the GRB host galaxies.

The optical light curves are usually composed of one or more power-law segments along with some humps, flares or rebrightening features (e.g. Li et al. 2012; Liang et al. 2013; Wang et al. 2013, 2015). To decompose the rich temporal features of GRB light curves, we fit the light curves with a model of multiple components. Similar to Wang et al. (2015), we decompose the lightcurves into several basic components, i.e. a single power-law (SPL)

function

$$F_1 = F_{01} t^{-\alpha}, \quad (1)$$

or a smooth broken power-law (BPL) function

$$F_2 = F_{02} \left[\left(\frac{t}{t_b} \right)^{\alpha_1 \omega} + \left(\frac{t}{t_b} \right)^{\alpha_2 \omega} \right]^{-1/\omega}, \quad (2)$$

where $\alpha, \alpha_1, \alpha_2$ are the temporal slopes, t_b is the break time, and ω measures the sharpness of the break, or a smooth triple-power-law (TPL) function that catches the canonical shape of X-ray lightcurves (Zhang et al. 2006; Nousek et al. 2006), i.e.

$$F_3 = (F_2^{-\omega_2} + F_4^{-\omega_2})^{-1/\omega_2} \quad (3)$$

where ω_2 is the sharpness factor of the second break at $t_{b,2}$, and

$$F_4 = F_2(t_{b,2}) \left(\frac{t}{t_{b,2}} \right)^{-\alpha_3}. \quad (4)$$

We perform best fits to the data using the subroutine MPFIT (Markwardt 2009). The sharpness parameter ω and ω_2 are usually adopted as 3 or 1 in our fitting. A minimum number of components (SPL, BPL, or TPL) are introduced initially based on eye inspection.

If the reduced χ^2 is much larger than 1, we then continue to add more components into the fitting, until the reduced χ^2 becomes close to 1 (usually less than 1.5). We'd like to stress that one may not solely based on χ^2 to evaluate whether a jet break is robust. This is because some GRBs (e.g., GRB 050730, 060729, 090926A) show erratic fluctuations in the lightcurves with small error bars. The reduced χ^2 values of these bursts are much larger than 1. Inspecting their light curves, the large χ^2 are caused by the complicated features in the light curves (such as small flares and fluctuations). However, the PL and BPL fits in any case catch the general features of these lightcurves. Even though adding more comments can reach better reduced χ^2 , we do not add them since we are not interested in the fine-details of the lightcurves. The χ^2 values of these fits remain much greater than 1. Furthermore, to avoid the additional features (e.g., steep decay phase, flares, re-brightening features) to affect the fits, we just perform the best fits in the time interval around the jet break. In some cases, the reduced χ^2 values for the lightcurve fittings are much smaller than 1. It means that some model parameters are poorly constrained. For these cases, we fix some parameters and redo the fits until the reduced χ^2 becomes close to 1. According to the MPFIT documentation, the error estimates produced by MPFITFUN/EXPR would not be correct if the data points

with large errors are not be properly weighted. In this case, we set the “Error” term to unity and proceed with the fit¹. We call the PERROR routine in the MPFITFUN to obtain the parameter errors, and use the 2σ parameter errors in our analysis.

3. Selection criteria and Jet Break Candidates

3.1. Jet break light curves

After the launch of the *Swift* satellite in 2004 (Gehrels et al. 2004), a rich data base of the light curves have been collected, which allowed a systematic analysis of the emission components of the broadband light curves, especially for the X-ray lightcurves (e.g. Barthelmy et al. 2005; Fan & Wei 2005; Tagliaferri et al. 2005; Zhang et al. 2006; Nousek et al. 2006; Liang et al. 2007, 2008; Racusin et al. 2009; Margutti et al. 2010) and the optical lightcurves (e.g. Liang et al. 2006; Nardini et al. 2006; Kann et al. 2006, 2010a, 2011; Panaitescu & Vestrand 2008, 2011; Li et al. 2012). “Synthetic” lightcurves of X-ray and optical emission have been summarized by Zhang et al. (2006) and Li et al. (2012). In both bands, one prominent feature in the late afterglow phase is the existence of a jet break feature. In principle, one can have two types of jet breaks (e.g. Wang et al. 2015):

- Standard jet break: This corresponds to the transition from the normal decay phase (standard afterglow component) to the post-jet-break phase in the canonical lightcurve. Lightcurves of such a category are caused by an edge-effect or with a contribution of sideways expansion. The post-break decay index is required to be steeper than 1.5 for this model. The post-break index can be as steep as the electron energy index p as predicted by the sideways expansion models (Sari et al. 1999).
- Jet break with energy injection: This corresponds to the case of an extended energy injection phase which extends to a duration longer than the jet break time. As a result, the jet break is expressed in terms of a shallow decay phase followed by a steeper decay phase with the break consistent with being due to a jet edge effect. Both before and after the break, the afterglow can be delineated by an afterglow model with a continuous energy injection defined by a long-lasting central engine activity history $L(t) = L_0(\frac{t}{t_0})^{-q}$ (Zhang & Mészáros 2001), where q is the energy injection parameter. In principle, energy injection can be interpreted as either a long-lasting central engine (Dai & Lu 1998; Zhang & Mészáros 2001) or a Lorentz-factor-stratified

¹<http://www.physics.wisc.edu/~craigm/idl/mpfittut.html>.

ejecta (Rees & Mészáros 1998; Sari & Mészáros 2000; Uhm et al. 2012). These two scenarios are equivalent with each other, and can be both delineated with the parameter q (Zhang et al. 2006).

3.2. Selection criteria

We make use of the standard synchrotron external shock models of GRB afterglow to select the jet break sample. The criteria are the relationship between the temporal index α and spectral index β (with the convention $F_\nu \propto t^{-\alpha}\nu^{-\beta}$) as predicted by various external shock models, known as the “closure relations” (e.g., Zhang & Mészáros 2004; Zhang et al. 2006; Gao et al. 2013). The indices α and β can be directly measured from the observational data. The predictions of the $\alpha - \beta$ relation depend on the sub-models (ISM vs. wind, adiabatic vs. radiative, whether or not there is energy injection, etc.), dynamical regimes (reverse shock crossing phase, self-similar deceleration phase, post-jet-break phase, Newtonian phase, etc.), and spectral regimes (different orders among the observed frequency (ν) and several characteristic frequencies (minimum injection frequency ν_m , cooling frequency ν_c , and self-absorption frequency ν_a). More details can be found in the comprehensive review by Gao et al. (2013). Generally, the optical band is in either the spectral regime $\nu > \nu_c$ (Regime I, $\beta = p/2$) or $\nu_m < \nu < \nu_c$ (Regime II, $\beta = (p-1)/2$) in the simplest analytical model (Sari et al. 1998). Due to the smoothness of the spectral breaks, the transition between the two regimes (regime I - II, $(p-1)/2 < \beta < p/2$) may take several orders of magnitude in observer time. This period may be defined as a “grey zone” (Zhang et al. 2006; Uhm & Zhang 2014), during which the $\alpha - \beta$ relation does not need to strictly satisfy the Regime I and Regime II regimes. The parameter space between the two closure relation lines is allowed by the theory. Data points falling into this grey zone should be regarded as consistent with the model.

We employ the $\alpha - \beta$ closure relations (Table 1) for the ISM ($k = 0$) or wind ($k = 2$) medium models and with or without energy injection. For a steepening break, we require that the same model applies to both pre- and post-break phase, with the post-break decay defined either by the edge effect of sideways expansion effect. We have assumed $\nu_a < \min(\nu_m, \nu_c)$ and $\nu_O > \nu_m$ (ν_O is the frequency of optical band), which is usually satisfied for optical afterglow emission for typical GRB parameters. A GRB to be included in our jet break sample needs to satisfy the following criteria:

- The optical lightcurves should satisfy closure relations of the same circumburst medium type (ISM or wind) in both pre- and post-break temporal segments, and the inferred

electron spectral index p from both pre- and post-break segments should be consistent with each other within error.

- For a jet break without energy injection, the light curves should satisfy the closure relations for the constant-energy ISM or wind models before the break, and the corresponding jet model for either edge or sideways expansion effect after the break.
- For a jet break with energy injection, the light curves should satisfy the closure relations for the energy-injection ISM or wind models in both pre- and post-break phases, with the energy injection q parameter consistent with each other within error.
- The X-ray afterglow lightcurves of these bursts are found to be consistent with the same jet break model, as have been studied in detail in Wang et al. (2015). We only plot X-ray lightcurves in Figure 1-3 for a self-consistency check, without repeating the closure relation analysis for X-rays.

For those GRBs that cannot be identified as jet break candidates with the $\alpha - \beta$ closure relation, we classify them as either lower limit or upper limit candidates. Some GRBs satisfy the $\alpha - \beta$ closure relations of pre-jet break phase, and no break is observed at the last observational data point. These bursts are included in the lower limit jet break sample. Some other GRBs have their temporal slopes steeper than the normal decay and satisfy the $\alpha - \beta$ closure relations of post-jet break phase. However, no jet break is identified at the first point of this lightcurve segment (there might be complicated components before that). We classify these as the upper limit jet break sample.

3.3. Jet break candidates

We find that 55 out of 99 GRBs can satisfy the jet break criteria. We then characterize these GRBs as the jet break candidates (as shown in Table 2 and Figure 1). Figure 4 shows the $\alpha - \beta$ values measured from the lightcurves as compared against the closure relations. Another 41 and 3 GRBs are classified as the candidates with the lower and upper limits of the jet break time, respectively (as shown in Table 3 - 4 and Figure 2 - 3).

Among the 55 jet break GRB candidates, 53 are Type II (long) GRBs and 2 are Type I (short) GRB (GRB 051221A, and 130603B). Three GRBs (GRB 080319B, 080413B, 090426) have two jet breaks and are consistent with the two-component jet model (e.g. Racusin et al. 2008; Nicuesa Guelbenzu et al. 2011a; Filgas et al. 2011). Only one GRB (GRB 030723) shows jet break with energy injection.

There are some GRBs that are consistent with more than one closure relation given their error bars. 53/55 and 40/55 GRBs can be consistent with ISM and wind model, respectively. The ISM model applies to more bursts than the wind model, which is consistent with the previous results (e.g., Panaiteescu & Kumar 2002; Yost et al. 2003; Zhang et al. 2006; Schulze et al. 2011; Wang et al. 2015). **38/55** GRBs are located in the grey zone between regime I and regime II. The median electron spectral index p of the jet break GRBs is $p = 2.39 \pm 0.48$ (Figure 6), which is very consistent with the previous studies (e.g., Achterberg et al. 2001; Ellison & Double 2002; Shen et al. 2006; Liang et al. 2007, 2008; Curran et al. 2010; Wang et al. 2015). The jet break time distribution can be roughly fit by a Gaussian function, with a typical value $t_b = 90.06 \pm 84.36$ ks (Figure 5). The early jet break for the two-component jets has a distribution of $t_b = 0.2 \sim 2$ ks (Figure 5).

4. Jet Angle Distribution and GRB Energetics

With the jet break time, one can calculate the half opening angle of the GRB jet, i.e.

$$\theta_j = 0.07 \text{ rad} \left(\frac{t_b}{1 \text{ day}} \right)^{3/8} \left(\frac{1+z}{2} \right)^{-3/8} \left(\frac{E_{\text{K,iso}}}{10^{53} \text{ ergs}} \right)^{-1/8} \left(\frac{n}{0.1 \text{ cm}^{-3}} \right)^{1/8} \quad (5)$$

for a constant density ISM medium (Rhoads 1999; Sari et al. 1999; Frail et al. 2001), and

$$\theta_j = 0.1 \text{ rad} \left(\frac{t_b}{1 \text{ day}} \right)^{1/4} \left(\frac{1+z}{2} \right)^{-1/4} \left(\frac{E_{\text{K,iso}}}{10^{53} \text{ ergs}} \right)^{-1/4} \left(\frac{A_*}{1 \text{ cm}^{-3}} \right)^{1/4} \quad (6)$$

for a wind medium (Chevalier & Li 2000; Bloom et al. 2003). Notice that θ_j depends on the isotropic kinetic energy of the blastwave, $E_{\text{K,iso}}$, rather than the isotropic γ -ray energy, $E_{\gamma,\text{iso}}$. In some works, θ_j is expressed in terms of $E_{\gamma,\text{iso}}$ through an efficiency parameter, which is assumed for a typical value. In order to more precisely estimate θ_j , in this work we infer $E_{\text{K,iso}}$ directly from the data.

The isotropic γ -ray energy $E_{\gamma,\text{iso}}$ of a GRB is calculated as

$$E_{\gamma,\text{iso}} = \frac{4\pi D_L^2 S_\gamma k}{1+z}, \quad (7)$$

where S_γ is the gamma-ray fluence in the instrument band, D_L is the luminosity distance of the source at redshift z , and the parameter k is a factor to correct the observed γ -ray energy in a given band pass to a broad band (e.g., $1 - 10^4$ keV in the rest frame) with the observed GRB spectra (Bloom et al. 2001). We assume a Band function shape of the GRB spectrum (Band et al. 1993) and use the fitted spectral parameters to do the extrapolation.

The isotropic kinetic energy $E_{K,\text{iso}}$ is calculated based on the standard afterglow models (Zhang et al. 2007; Gao et al. 2013; Wang et al. 2015). More specifically we use Equations (13-41) of Wang et al. (2015) to calculate $E_{K,\text{iso}}$ based on the medium type, spectral regime, and the value of p (> 2 or < 2) inferred from the data. Since the optical band is typically in the regime $\nu_m < \nu < \nu_c$, we adopt Eqs. (20), (25), (34) and (39) of Wang et al. (2015) to perform the calculations. If the GRB is consistent with more than one closure relation, we choose the ISM model for the calculation of jet angles and energetics. The model parameters are taken as typical values: $\epsilon_e = 0.1$, $\epsilon_B = 10^{-5}$, $n = 1$ or $A_* = 1$, and $Y = 1$ (Wang et al. 2015).

With inferred θ_j , one can derive the geometrically corrected γ -ray energy

$$E_\gamma = f_b E_{\gamma,\text{iso}} = (1 - \cos \theta_j) E_{\gamma,\text{iso}}, \quad (8)$$

and kinetic energy

$$E_K = f_b E_{K,\text{iso}} = (1 - \cos \theta_j) E_{K,\text{iso}}, \quad (9)$$

through the beaming correction factor defined as

$$f_b = (1 - \cos \theta_j). \quad (10)$$

For all the bursts in this sample, we collect the measured z and E_p from the literature (as listed in Tables 2-4). We derive jet angles and energetics of GRBs using the available z and E_p . Within the jet break, lower limit, and upper limit samples, 50, 38 and 3 GRBs have measured z from the literature, respectively. Since *Swift*-BAT has a narrow energy bandpass, the best fit spectrum is generally a power-law. The E_p values derived from the *Swift*-BAT data alone are limited, since E_p may be measured only when it falls approximately between 15 and 150 keV. In our sample, we only adopted the E_p derived from *Swift*-BAT for GRB 050416A (Sakamoto et al. 2005b; Nava et al. 2008, 2012), 050502A (Nava et al. 2008, 2012) and 060206 (Cenko et al. 2006; Nava et al. 2008, 2012). If there are multiple instruments/missions (e.g., *CGRO*-BATSE, *Fermi*-GBM, *HETE*-2-FREGATE, *INTEGRAL*-SPI/IBIS, *Konus*-Wind, *RHESSI*, *Suzaku*-WAM) that detected a same burst, the instruments/missions with the best fit Band function spectrum are adopted as the source of E_p and S_γ (also listed in Tables 2-4).

Our data suggest $\theta_j = (2.5 \pm 1.0)^\circ$ (as shown in Figure 8), and the typical jet beaming factor $f_b^{-1} \sim 1000$. Notice that the typical jet half opening angle is smaller than the value ($\sim 5^\circ$) inferred before (e.g. Frail et al. 2001; Bloom et al. 2003). The main reason is that recent studies have suggested a relatively small value of ϵ_B , of the order of $10^{-5} - 10^{-7}$ (e.g. Kumar & Barniol Duran 2009; Santana et al. 2014; Wang et al. 2015; Gao & Zhang 2015a; Zhang et al. 2015), which suggests a relatively larger $E_{K,\text{iso}}$ than estimated before assuming

a fixed GRB efficiency². The smaller half jet opening angle also suggests a smaller beaming correction factor f_b^{-1} , suggesting a somewhat higher event rate density of GRB progenitor systems.

Figure 9 shows the radiative efficiency calculated at t_b . Most GRBs show a small radiative efficiency with less than 10%. With a smaller value of $\epsilon_B \sim 10^{-5}$, the derived $E_{K,\text{iso}}$ values are systematically larger, so that the derived efficiency values are somewhat smaller than the values derived in previous work (e.g. Zhang et al. 2007; Racusin et al. 2011). Nonetheless, the efficiency derived at the end of prompt emission (beginning of the shallow decay case) remain tens of percent for most GRBs, which demands a contrived setup for the internal shock models (e.g., Beloborodov 2000; Kobayashi & Sari 2001; Zhang & Yan 2011; Deng et al. 2015; Gao & Zhang 2015b).

Table 5 and Figure 7 displays the inferred mean value of various energies. For Type II GRBs, one has $\log(E_{\gamma,\text{iso}}/\text{erg}) = 53.11 \pm 0.84$, $\log(E_{K,\text{iso}}/\text{erg}) = 54.82 \pm 0.56$, $\log(E_{\gamma}/\text{erg}) = 49.54 \pm 1.29$, and $\log(E_K/\text{erg}) = 51.33 \pm 0.58$. For Type I GRBs, the energies are typically lower, i.e. $\log(E_{\gamma,\text{iso}}/\text{erg}) \sim 51$, $\log(E_{K,\text{iso}}/\text{erg}) \sim 53$, $\log(E_{\gamma}/\text{erg}) \sim 49$ and $\log(E_K/\text{erg}) \sim (50 - 51)$.

The results of the lower limit and upper limit samples are presented in Table 6 - 7 and Figure 7 - 9. For the lower limit sample, the epoch of last data point is used to calculate the lower limit of the jet opening angle. For the upper limit sample, the first data point that marks the transition to the post-jet break phase (from a complicated component, e.g. flare) is used to set the upper limit of the jet opening angle (as shown in Figure 3).

5. Luminosity Correlations

In order to investigate several GRB luminosity correlations claimed in previous papers, we compile the necessary parameters of the GRBs in our sample in Table 2. Their derived parameters are presented in Table 5.

We test four correlations, i.e. the $E_{p,z} - E_{\gamma,\text{iso}}$ (*Amati*) (Amati et al. 2002; Amati 2006), $E_{p,z} - E_{\gamma}$ (*Ghirlanda*) (Ghirlanda et al. 2004), $E_{p,z} - E_{\gamma,\text{iso}} - t_{b,z}$ (*Liang-Zhang*) (Liang & Zhang 2005), and $E_{\gamma,\text{iso}} - f_b$ (*Frail*) (Frail et al. 2001) relations. We write the

² Zhang et al. (2015) focused on GRBs with long-lasting X-ray light curves that require very late-time *Chandra* observations, and therefore selected against bursts with small jet opening angles.

correlations of $E_{\text{p,z}} - E_{\gamma,\text{iso}}$ (*Amati*) or $E_{\text{p,z}} - E_{\gamma}$ (*Ghirlanza*) in the form of

$$\frac{E_{\text{p,z}}}{100\text{keV}} = C \left(\frac{E_{\gamma,\text{iso}}(E_{\gamma})}{10^{52}\text{erg}} \right)^a, \quad (11)$$

and the $E_{\text{p,z}} - E_{\gamma,\text{iso}} - t_{\text{b,z}}$ correlation (*Liang-Zhang*) in the form of

$$\frac{E_{\text{p,z}}}{100\text{keV}} = C \left(\frac{E_{\gamma,\text{iso}}}{10^{52}\text{erg}} \right)^a \left(\frac{t_{\text{b,z}}}{\text{day}} \right)^b, \quad (12)$$

where $E_{\text{p,z}}$ and $t_{\text{b,z}}$ are the peak energy and jet break time in the rest-frame with $E_{\text{p,z}} = (1+z)E_p$ and $t_{\text{b,z}} = t_b/(1+z)$, respectively; C , a and b are the correlation indices. When conducting both single and multiple variable regression analyses to look for correlations, one may find discrepancy of the dependencies among variables by specifying different dependent variables for a given data set, especially when the data have large error bars or large scatter. To avoid specifying independent and dependent variables in the best linear fits, in principle the algorithm of the bisector of two ordinary least-squares may be adopted. We therefore use the Spearman correlation analysis to search for correlations among these parameters, and adopt the stepwise regression analysis method to perform a multiple regression analysis for multiple parameters (Liang et al. 2015).

Type II GRBs in our sample can be fit with a tight *Amati* relation, with $\frac{E_{\text{p,z}}}{100\text{keV}} \simeq (0.63 \pm 0.31) \left(\frac{E_{\gamma,\text{iso}}}{10^{52}\text{erg}} \right)^{(0.69 \pm 0.07)}$ (Table 8 and Figure 10). The previous studies suggested that $C \sim (0.8 - 1)$ and $m \sim (0.4 - 0.6)$ (Amati et al. 2002; Amati 2006; Sakamoto et al. 2006; Frontera et al. 2012). Our slope is slightly steeper. One GRB (GRB 120729A) deviates from the relation. Type I GRBs (GRB 051221A and 1306033B) generally deviate from this relation with a relative low energy and high $E_{\text{p,z}}$.

The $E_{\text{p,z}} - E_{\gamma}$ (*Ghirlanza*) (Table 8 and Figure 11) has large scatter, with $\frac{E_{\text{p,z}}}{100\text{keV}} \simeq (7.9 \pm 4.8) \left(\frac{E_{\gamma}}{10^{51}\text{erg}} \right)^{(0.44 \pm 0.17)}$. Even though the results are generally consistent with Ghirlanza et al. (2004), $\frac{E_{\text{p,z}}}{100\text{keV}} \simeq 8 \left(\frac{E_{\gamma}}{10^{51}\text{erg}} \right)^{0.7}$, the large dispersion in the normalization parameter C suggests that it is not as tight as claimed before. We separate our sample to GRBs with jet break time earlier and later than 10^4 s, and found that they are well separated in the $E_{\text{p,z}} - E_{\gamma}$ plane. Limiting the sample to the late jet break ones, one gets a tighter *Ghirlanza*-relation.

Similar to *Ghirlanza* relation, the early time jet break GRBs also introduce scatter to the $E_{\text{p,z}} - E_{\gamma,\text{iso}} - t_{\text{b,z}}$ (*Liang-Zhang*) correlation. Limiting to the late jet break sample, we get a tight $E_{\text{p,z}} - E_{\gamma,\text{iso}} - t_{\text{b,z}}$ relation, $\frac{E_{\text{p,z}}}{100\text{keV}} = (1.2 \pm 0.3) \left(\frac{E_{\gamma,\text{iso}}}{10^{52}\text{erg}} \right)^{(0.56 \pm 0.07)} \left(\frac{t_{\text{b,z}}}{\text{day}} \right)^{(0.67 \pm 0.08)}$. The correlation coefficient is 0.85 and the dispersion is $\delta = 0.15$ with a chance probability $p < 10^{-4}$ (Table 8 and Figure 12). This is a tight correlation as claimed by Liang & Zhang (2005). Including early jet breaks, the correlation is less tight with $\frac{E_{\text{p,z}}}{100\text{keV}} =$

$(1.3 \pm 0.4) \left(\frac{E_{\gamma, \text{iso}}}{10^{52} \text{erg}} \right)^{(0.49 \pm 0.07)} \left(\frac{t_{\text{b,z}}}{\text{day}} \right)^{(-0.08 \pm 0.05)}$, and regression leads to a correlation with different indices, i.e. correlation coefficient ~ 0.67 , dispersion $\sim \delta = 0.22$ and chance probability $p < 10^{-4}$.

The $E_{\gamma, \text{iso}} - f_b$ relation (*Frail*) remains loose (Figure 13(a)). We also extend it to $E_{\text{K,iso}} - f_b$ (Berger et al. 2003) (Figure 13(b)). Limiting to Type II GRBs, we get a scatter relation with $E_{\text{K,iso}} \propto f_b^{-0.8}$.

6. Conclusions and Discussion

The collimation of GRB jets is an important subject, and there have been many investigations in the past. After more than 10 years of successful operation of the *Swift* satellite, the sample of GRB afterglow expands significantly. It is therefore justified to revisit the jet break problem with a much larger sample, especially with the bursts with multi-wavelength data to confirm the predicted achromatic feature of jet breaks. In this paper, we have systematically studied the optical jet breaks of all the GRBs detected from February 1997 to March 2015, with most of them having X-ray data showing the consistency with the achromatic prediction. Making use of the standard external shock model, we identified 55 out of 99 GRBs that display a clear jet break in the optical light curves, which include 53 type II and 2 type I GRBs. Among them 3 GRBs show two jet breaks, 1 GRBs show jet break with energy injection.

Some interesting conclusions are obtained from our analysis:

- Most GRBs in the jet break sample are generally consistent with the ISM model. Only one jet break with energy injection is identified, suggesting that the time when energy injection ceases is typically earlier than the jet break time³.
- The jet break time has a distribution $t_b = 90.06 \pm 84.36$ ks, which gives a jet half-opening-angle distribution $\theta_j = (2.5 \pm 1.0)^\circ$ and the beaming correction factor $\log f_b^{-1} = 3.00 \pm 0.48$. The typical angle is smaller than the previous claimed 5° , which is caused by a more general treatment of the afterglow kinetic energy, which is derived to be larger due to the small ϵ_B inferred by many recent studies.
- The typical jet correction factor $f_b^{-1} \sim 1000$ is larger than the previously inferred

³ Similar to X-ray lightcurves that usually show an early shallow decay phase (Zhang et al. 2006; Nousek et al. 2006), a shallow decay phase is also seen in the optical band in some GRBs (Li et al. 2012; Wang et al. 2015), which requires energy injection into the blastwave.

values (Frail et al. 2001; Guetta et al. 2005; Liang et al. 2007; Racusin et al. 2009), suggesting a factor of two higher event rate density of GRB events.

- With the inferred jet opening angles, one can derive the distributions of various energies, which read $\log(E_{\gamma,\text{iso}}/\text{erg}) = 53.11 \pm 0.84$, $\log(E_{K,\text{iso}}/\text{erg}) = 54.82 \pm 0.56$, $\log(E_{\gamma}/\text{erg}) = 49.54 \pm 1.29$ and $\log(E_K/\text{erg}) = 51.33 \pm 0.58$. They generally all have large scatter, even for jet corrected values. This suggests that GRBs do not have a standard energy reservoir as speculated before.
- The derived electron spectral index has a distribution $p = 2.39 \pm 0.48$, which is consistent with earlier results.
- A fraction of GRBs have lower limits of jet break time. However, due to the sensitivity limits, these lower limits are generally consistent with the observed jet break time distribution. The typical jet half-opening-angle of the true distribution may be consistent with or somewhat larger than the value inferred from this paper.

We also revisited several previously claimed luminosity correlations. Following results are obtained:

- $E_{p,z} - E_{\gamma,\text{iso}}$ (*Amati* relation): The relation remains tight even though with a slightly steeper power law index, i.e. $\frac{E_{p,z}}{100\text{keV}} \simeq (0.63 \pm 0.31) \left(\frac{E_{\gamma,\text{iso}}}{10^{52}\text{erg}} \right)^{(0.69 \pm 0.07)}$.
- $E_{p,z} - E_{\gamma}$ (*Ghirlanza* relation): This relation has much larger scatter than claimed before, i.e. $\frac{E_{p,z}}{100\text{keV}} \simeq (7.9 \pm 4.8) \left(\frac{E_{\gamma}}{10^{51}\text{erg}} \right)^{(0.44 \pm 0.17)}$. The existence of early jet breaks discovered in the *Swift* era is likely the origin of the scatter.
- $E_{p,z} - E_{\gamma,\text{iso}} - t_{b,z}$ (*Liang-Zhang* relation): Similar to the *Ghirlanza* relation, early jet breaks introduce significant scatter to the correlation. Limited to the late jet break sample ($t_b > 10^4$ s), the correlation remains tight, i.e. $\frac{E_{p,z}}{100\text{keV}} = (1.2 \pm 0.3) \left(\frac{E_{\gamma,\text{iso}}}{10^{52}\text{erg}} \right)^{(0.56 \pm 0.07)} \left(\frac{t_{b,z}}{\text{day}} \right)^{(0.67 \pm 0.08)}$. Including early jet breaks, the correlation is less tight with $\frac{E_{p,z}}{100\text{keV}} = (1.3 \pm 0.4) \left(\frac{E_{\gamma,\text{iso}}}{10^{52}\text{erg}} \right)^{(0.49 \pm 0.07)} \left(\frac{t_{b,z}}{\text{day}} \right)^{(-0.08 \pm 0.05)}$.
- $E_{\gamma} - f_b$ (*Frail* relation): Both $E_{\gamma,\text{iso}} - f_b$ and $E_{K,\text{iso}} - f_b$ relations have very large scatter, suggesting that GRBs do not have a standard energy reservoir.
- Type I GRBs usually deviate from these correlations, which are derived from Type II GRBs.

We note that there are jet breaks happening in the early time in the optical band, e.g., GRB 051111 ~ 2.7 ks, GRB 070419A ~ 1.5 ks, GRB 080413A ~ 1 ks, GRB 120729A ~ 5.6

ks. The t_b of the first jet break in the two-component jets are $0.2 \sim 2$ ks. Usually, the data between $\sim 1 \sim 3$ ks are missed in the XRT, which may bury the early jet break phenomena. The results are differ from the observational strategies for searching GRBs jet break, which are focused on the late time afterglows (e.g. Zhang et al. 2015). In the past few years, *swift* has changed their GRB follow-up strategies, generally following GRBs for a lot less duration than earlier in the mission. However, there is not much change since optical observers only need the accurate position of GRBs, which usually provided by XRT.

The GRBs studied in this paper are chosen to have both measure X-ray and optical afterglows and their spectral indices. In order to study their energetics, redshift information is needed. As a result, the studied sample is a small fraction of all the detected GRBs, especially for short GRBs and low-luminosity GRBs. In order to address many open questions in GRB physics (e.g. Zhang 2011), such as GRB prompt emission and afterglow physics, central engine, cosmological setting, more advanced multi-wavelength instruments with higher sensitivity, larger field of view, and wider energy bandpass are needed. Many in-progress observational facilities such as, Space-based Variable Objects Monitor (SVOM) (Wei et al. 2016), Advanced Telescope for High ENergy Astrophysics (ATHENA) (Nandra et al. 2013), The Transient High Energy Sources and Early Universe Surveyor (THESEUS) (Amati et al. 2017), enhanced X-ray Timing and Polarimetry mission (eXTP) (Zhang et al. 2016), Einstein Telescope (Hild et al. 2008), Transient Astrophysics Observer on the International Space Station (ISS-TAO)⁴, and Transient Astrophysics Probe (TAP)⁵, will usher in an exciting era of GRB study.

We thank an anonymous referee for helpful suggestions. This work is supported by the National Basic Research Program (973 Programme) of China (Grant No. 2014CB845800), the National Natural Science Foundation of China (Grants 11673006, 11533003, 11303005), the Guangxi Science Foundation (2016GXNSFFA380006, AD17129006).

⁴ <https://heasarc.gsfc.nasa.gov/docs/heasarc/missions/concepts.html>

⁵ <https://asd.gsfc.nasa.gov/tap/index.html>

REFERENCES

- Achterberg, A., Gallant, Y. A., Kirk, J. G., & Guthmann, A. W. 2001, MNRAS, 328, 393
- Afonso, P., Greiner, J., Pian, E., et al. 2011, A&A, 526, A154
- Amati, L. 2006, MNRAS, 372, 233
- Amati, L., Guidorzi, C., Frontera, F., et al. 2008, MNRAS, 391, 577
- Amati, L., Frontera, F., Tavani, M., et al. 2002, A&A, 390, 81
- Amati, L., O'Brien, P., Goetz, D., et al. 2017, ArXiv e-prints, arXiv:1710.04638
- Band, D., Matteson, J., Ford, L., et al. 1993, ApJ, 413, 281
- Barthelmy, S. D., Cannizzo, J. K., Gehrels, N., et al. 2005, ApJ, 635, L133
- Barthelmy, S. D., Cummings, J., Fenimore, E., et al. 2008, GRB Coordinates Network, 7447
- Beloborodov, A. M. 2000, ApJ, 539, L25
- Berger, E. 2014, ARA&A, 52, 43
- Berger, E., Kulkarni, S. R., & Frail, D. A. 2003, ApJ, 590, 379
- Bloom, J. S., Foley, R. J., Kocevski, D., & Perley, D. 2006, GRB Coordinates Network, 5217
- Bloom, J. S., Frail, D. A., & Kulkarni, S. R. 2003, ApJ, 594, 674
- Bloom, J. S., Frail, D. A., & Sari, R. 2001, AJ, 121, 2879
- Burrows, D. N., & Racusin, J. 2006, Nuovo Cimento B Serie, 121, 1273
- Burrows, D. N., Grupe, D., Capalbi, M., et al. 2006, ApJ, 653, 468
- Butler, N. R., Bloom, J. S., & Poznanski, D. 2010, ApJ, 711, 495
- Butler, N. R., Kocevski, D., Bloom, J. S., & Curtis, J. L. 2007, ApJ, 671, 656
- Cano, Z., de Ugarte Postigo, A., Pozanenko, A., et al. 2014a, A&A, 568, A19
- . 2014b, A&A, 568, A19
- Cenko, S. B., Bloom, J. S., Morgan, A. N., & Perley, D. A. 2009a, GRB Coordinates Network, 9053

- Cenko, S. B., Gezari, S., Small, T., Fox, D. B., & Chornock, R. 2007, GRB Coordinates Network, 6322
- Cenko, S. B., Hora, J. L., & Bloom, J. S. 2011, GRB Coordinates Network, Circular Service, No. 11638, #1 (2011), 11638
- Cenko, S. B., Perley, D. A., Junkkarinen, V., et al. 2009b, GRB Coordinates Network, 9518
- Cenko, S. B., Kasliwal, M., Harrison, F. A., et al. 2006, ApJ, 652, 490
- Chevalier, R. A., & Li, Z.-Y. 2000, ApJ, 536, 195
- Chornock, R., Berger, E., Fox, D., et al. 2010, GRB Coordinates Network, Circular Service, No. 11164, #1 (2010), 11164
- Chornock, R., Perley, D. A., Cenko, S. B., & Bloom, J. S. 2009a, GRB Coordinates Network, 9028
- Chornock, R., Perley, D. A., & Cobb, B. E. 2009b, GRB Coordinates Network, Circular Service, No. 10100, #1 (2009), 10100
- Collazzi, A. C. 2012, GRB Coordinates Network, Circular Service, No. 13145, #1 (2012), 13145
- Cucchiara, A., Fox, D., Levan, A., & Tanvir, N. 2009, GRB Coordinates Network, Circular Service, No. 10202, #1 (2009), 10202
- Cucchiara, A., & Fox, D. B. 2010, GRB Coordinates Network, Circular Service, No. 10624, #1 (2010), 10624
- Cucchiara, A., Cenko, S. B., Bloom, J. S., et al. 2011, ApJ, 743, 154
- Curran, P. A., Evans, P. A., de Pasquale, M., Page, M. J., & van der Horst, A. J. 2010, ApJ, 716, L135
- Curran, P. A., van der Horst, A. J., & Wijers, R. A. M. J. 2008, MNRAS, 386, 859
- Dai, X., Halpern, J. P., Morgan, N. D., et al. 2007, ApJ, 658, 509
- Dai, X., Garnavich, P. M., Prieto, J. L., et al. 2008, ApJ, 682, L77
- Dai, Z. G., & Lu, T. 1998, A&A, 333, L87
- D'Avanzo, P., D'Elia, V., & Covino, S. 2008, GRB Coordinates Network, 8350

- de Pasquale, M., Oates, S. R., Page, M. J., et al. 2007, MNRAS, 377, 1638
- de Pasquale, M., Evans, P., Oates, S., et al. 2009, MNRAS, 392, 153
- de Ugarte Postigo, A., Gorosabel, J., Fynbo, J. P. U., Wiersema, K., & Tanvir, N. 2009a, GRB Coordinates Network, 9771
- de Ugarte Postigo, A., Jakobsson, P., Malesani, D., et al. 2009b, GRB Coordinates Network, 8766
- D'Elia, V., Fiore, F., Perna, R., et al. 2009, ApJ, 694, 332
- Deng, W., Li, H., Zhang, B., & Li, S. 2015, ApJ, 805, 163
- Ellison, D. C., & Double, G. P. 2002, Astroparticle Physics, 18, 213
- Evans, P. A., Beardmore, A. P., Page, K. L., et al. 2009, MNRAS, 397, 1177
- Fan, Y. Z., & Wei, D. M. 2005, MNRAS, 364, L42
- Ferrero, P., Klose, S., Kann, D. A., et al. 2009, A&A, 497, 729
- Filgas, R., Krühler, T., Greiner, J., et al. 2011, A&A, 526, A113
- Firmani, C., Ghisellini, G., Avila-Reese, V., & Ghirlanda, G. 2006, MNRAS, 370, 185
- Fong, W., Berger, E., Margutti, R., et al. 2012, ApJ, 756, 189
- Fong, W., Berger, E., Metzger, B. D., et al. 2014, ApJ, 780, 118
- Fox, D. B., Berger, E., Price, P. A., & Cenko, S. B. 2007, GRB Coordinates Network, 6071
- Fratil, D. A., Kulkarni, S. R., Sari, R., et al. 2001, ApJ, 562, L55
- Frederiks, D. D., Hurley, K., Svinkin, D. S., et al. 2013, ApJ, 779, 151
- Frontera, F., Amati, L., Guidorzi, C., Landi, R., & in't Zand, J. 2012, ApJ, 757, 107
- Fugazza, D., D'Avanzo, P., Malesani, D., et al. 2006, GRB Coordinates Network, 5513
- Fynbo, J. P. U., Jakobsson, P., Jensen, B. L., et al. 2006, GRB Coordinates Network, 5651
- Fynbo, J. P. U., Jakobsson, P., Prochaska, J. X., et al. 2009, ApJS, 185, 526
- Gao, H., Lei, W.-H., Zou, Y.-C., Wu, X.-F., & Zhang, B. 2013, New A Rev., 57, 141
- Gao, H., & Zhang, B. 2015a, ApJ, 801, 103

- . 2015b, ApJ, 801, 103
- Gao, W.-H., & Wei, D.-M. 2005, Chinese J. Astron. Astrophys., 5, 571
- Gao, Y., & Dai, Z.-G. 2010, Research in Astronomy and Astrophysics, 10, 142
- Gehrels, N., Chincarini, G., Giommi, P., et al. 2004, ApJ, 611, 1005
- Gehrels, N., Sarazin, C. L., O'Brien, P. T., et al. 2005, Nature, 437, 851
- Gendre, B., Stratta, G., Laas-Bourez, M., et al. 2011, A&A, 530, A74
- Ghirlanda, G., Ghisellini, G., & Lazzati, D. 2004, ApJ, 616, 331
- Golenetskii, S., Aptekar, R., Mazets, E., et al. 2005a, GRB Coordinates Network, 3179
- . 2005b, GRB Coordinates Network, 4183
- . 2005c, GRB Coordinates Network, 4238
- . 2005d, GRB Coordinates Network, 4394
- . 2006a, GRB Coordinates Network, 5722
- . 2007, GRB Coordinates Network, 6849
- . 2008a, GRB Coordinates Network, 7482
- . 2008b, GRB Coordinates Network, 7487
- . 2006b, GRB Coordinates Network, 4989
- . 2008c, GRB Coordinates Network, 8611
- . 2009a, GRB Coordinates Network, 8776
- . 2009b, GRB Coordinates Network, 9030
- . 2011, GRB Coordinates Network, Circular Service, No. 11659, #1 (2011), 11659
- Golenetskii, S., Aptekar, R., Frederiks, D., et al. 2013, GRB Coordinates Network, Circular Service, No. 14487, #1 (2013), 14487
- Gorbovskoy, E. S., Lipunova, G. V., Lipunov, V. M., et al. 2012, MNRAS, 421, 1874
- Gorosabel, J., Castro-Tirado, A. J., Ramirez-Ruiz, E., et al. 2006, ApJ, 641, L13

- Granot, J., & Piran, T. 2012, MNRAS, 421, 570
- Greiner, J., Kröhler, T., Klose, S., et al. 2011, A&A, 526, A30
- Groot, P., Kaper, L., Ellerbroek, L., et al. 2010, GRB Coordinates Network, Circular Service, No. 10441, #1 (2010), 10441
- Grupe, D., Burrows, D. N., Patel, S. K., et al. 2006, ApJ, 653, 462
- Grupe, D., Gronwall, C., Wang, X.-Y., et al. 2007, ApJ, 662, 443
- Guetta, D., Granot, J., & Begelman, M. C. 2005, ApJ, 622, 482
- Guetta, D., Pian, E., & Waxman, E. 2011a, A&A, 525, A53
- . 2011b, A&A, 525, A53
- Guidorzi, C., Gomboc, A., Kobayashi, S., et al. 2007, A&A, 463, 539
- Guidorzi, C., Kobayashi, S., Perley, D. A., et al. 2011, MNRAS, 417, 2124
- Halpern, J. P., Uglesich, R., Mirabal, N., et al. 2000, ApJ, 543, 697
- Hild, S., Chelkowski, S., & Freise, A. 2008, ArXiv e-prints, arXiv:0810.0604
- Huang, Y. F., Gou, L. J., Dai, Z. G., & Lu, T. 2000, ApJ, 543, 90
- Jakobsson, P., Fynbo, J. P. U., Vreeswijk, P. M., Malesani, D., & Sollerman, J. 2007a, GRB Coordinates Network, 7076
- Jakobsson, P., Levan, A., Chapman, R., et al. 2006a, GRB Coordinates Network, 5617
- Jakobsson, P., Malesani, D., Thoene, C. C., et al. 2007b, GRB Coordinates Network, 6283
- Jakobsson, P., Vreeswijk, P., Fynbo, J. P. U., et al. 2006b, GRB Coordinates Network, 5320
- Jakobsson, P., Malesani, D., Vreeswijk, P. M., et al. 2008, GRB Coordinates Network, 7998
- Jaunsen, A. O., Malesani, D., Fynbo, J. P. U., Sollerman, J., & Vreeswijk, P. M. 2007a, GRB Coordinates Network, 6010
- Jaunsen, A. O., Thoene, C. C., Fynbo, J. P. U., Hjorth, J., & Vreeswijk, P. 2007b, GRB Coordinates Network, 6202
- Jaunsen, A. O., Hjorth, J., Björnsson, G., et al. 2001, ApJ, 546, 127

- Jia, L.-W., Wu, X.-F., Lü, H.-J., Hou, S.-J., & Liang, E.-W. 2012, Research in Astronomy and Astrophysics, 12, 411
- Jimenez, R., Band, D., & Piran, T. 2001, ApJ, 561, 171
- Jin, Z. P., Yan, T., Fan, Y. Z., & Wei, D. M. 2007, ApJ, 656, L57
- Kamble, A., Misra, K., Bhattacharya, D., & Sagar, R. 2009, MNRAS, 394, 214
- Kann, D. A., Klose, S., & Zeh, A. 2006, ApJ, 641, 993
- Kann, D. A., Klose, S., Zhang, B., et al. 2010a, ApJ, 720, 1513
- . 2010b, ApJ, 720, 1513
- . 2011, ApJ, 734, 96
- Kobayashi, S., & Sari, R. 2001, ApJ, 551, 934
- Kocevski, D., & Butler, N. 2008, ApJ, 680, 531
- Kouveliotou, C., Meegan, C. A., Fishman, G. J., et al. 1993, ApJ, 413, L101
- Krinn, H. A., Yamaoka, K., Sugita, S., et al. 2009, ApJ, 704, 1405
- Krühler, T., Greiner, J., McBreen, S., et al. 2009a, ApJ, 697, 758
- Krühler, T., Greiner, J., Afonso, P., et al. 2009b, A&A, 508, 593
- Kumar, P., & Barniol Duran, R. 2009, MNRAS, 400, L75
- Kumar, P., & Zhang, B. 2015, Phys. Rep., 561, 1
- Landsman, W., de Pasquale, M., Kuin, P., et al. 2008, GRB Coordinates Network, 8601
- Levan, A. J., Cenko, S. B., Perley, D. A., & Tanvir, N. R. 2013, GRB Coordinates Network, Circular Service, No. 14455, #1 (2013), 14455
- Levan, A. J., Tanvir, N. R., Wiersema, K., Berger, E., & Fox, D. 2011, GRB Coordinates Network, Circular Service, No. 12368, #1 (2011), 12368
- Levesque, E., Chornock, R., Kewley, L., et al. 2009, GRB Coordinates Network, 9264
- Li, L., Liang, E.-W., Tang, Q.-W., et al. 2012, ApJ, 758, 27
- Liang, E., & Zhang, B. 2005, ApJ, 633, 611

- . 2006, ApJ, 638, L67
- Liang, E.-W., Lin, T.-T., Lü, J., et al. 2015, ApJ, 813, 116
- Liang, E.-W., Racusin, J. L., Zhang, B., Zhang, B.-B., & Burrows, D. N. 2008, ApJ, 675, 528
- Liang, E.-W., Zhang, B.-B., & Zhang, B. 2007, ApJ, 670, 565
- Liang, E. W., Zhang, B., O'Brien, P. T., et al. 2006, ApJ, 646, 351
- Liang, E.-W., Li, L., Gao, H., et al. 2013, ApJ, 774, 13
- Malesani, D., Schulze, S., de Ugarte Postigo, A., et al. 2012, GRB Coordinates Network, Circular Service, No. 13649, #1 (2012), 13649
- Malesani, D., Goldoni, P., Fynbo, J. P. U., et al. 2009, GRB Coordinates Network, 9942
- Mannucci, F., Salvaterra, R., & Campisi, M. A. 2011, MNRAS, 414, 1263
- Margutti, R., Guidorzi, C., Chincarini, G., et al. 2010, MNRAS, 406, 2149
- Markwardt, C. B. 2009, in Astronomical Society of the Pacific Conference Series, Vol. 411, Astronomical Data Analysis Software and Systems XVIII, ed. D. A. Bohlender, D. Durand, & P. Dowler, 251
- Martin-Carrillo, A., Hanlon, L., Topinka, M., et al. 2014, A&A, 567, A84
- Mészáros, P., & Rees, M. J. 1997, ApJ, 476, 232
- Nandra, K., Barret, D., Barcons, X., et al. 2013, ArXiv e-prints, arXiv:1306.2307
- Nardini, M., Ghisellini, G., Ghirlanda, G., et al. 2006, A&A, 451, 821
- Nava, L., Ghirlanda, G., Ghisellini, G., & Firmani, C. 2008, MNRAS, 391, 639
- Nava, L., Ghisellini, G., Ghirlanda, G., et al. 2007, MNRAS, 377, 1464
- Nava, L., Salvaterra, R., Ghirlanda, G., et al. 2012, MNRAS, 421, 1256
- Nicuesa Guelbenzu, A., Klose, S., Rossi, A., et al. 2011a, A&A, 531, L6
- . 2011b, A&A, 531, L6
- Nicuesa Guelbenzu, A., Klose, S., Krühler, T., et al. 2012, A&A, 538, L7

- Nousek, J. A., Kouveliotou, C., Grupe, D., et al. 2006, ApJ, 642, 389
- Ohno, M., Kokubun, M., Suzuki, M., et al. 2008, GRB Coordinates Network, 7630
- Paczyński, B. 1998, ApJ, 494, L45
- Pal’Shin, V., Golenetskii, S., Aptekar, R., et al. 2008, GRB Coordinates Network, 8256
- Panaiteescu, A. 2005a, MNRAS, 363, 1409
- . 2005b, MNRAS, 362, 921
- . 2007, MNRAS, 380, 374
- Panaiteescu, A., & Kumar, P. 2002, ApJ, 571, 779
- Panaiteescu, A., & Vestrand, W. T. 2008, MNRAS, 387, 497
- . 2011, MNRAS, 414, 3537
- Perley, D. A., Bloom, J. S., & Prochaska, J. X. 2008a, GRB Coordinates Network, 7791
- Perley, D. A., Chornock, R., & Bloom, J. S. 2008b, GRB Coordinates Network, 7962
- Perley, D. A., Li, W., Chornock, R., et al. 2008c, ApJ, 688, 470
- Perley, D. A., Bloom, J. S., Butler, N. R., et al. 2008d, ApJ, 672, 449
- Perley, D. A., Cenko, S. B., Corsi, A., et al. 2014, ApJ, 781, 37
- Price, P. A., Bloom, J. S., Goodrich, R. W., et al. 2002, GRB Coordinates Network, 1475
- Price, P. A., Cowie, L. L., Minezaki, T., et al. 2006, ApJ, 645, 851
- Price, P. A., Kulkarni, S. R., Berger, E., et al. 2003, ApJ, 589, 838
- Prochaska, J. X., Foley, R. J., Holden, B., et al. 2008, GRB Coordinates Network, 7397
- Prochaska, J. X., Chen, H.-W., Bloom, J. S., et al. 2007, ApJS, 168, 231
- Racusin, J. L., Karpov, S. V., Sokolowski, M., et al. 2008, Nature, 455, 183
- Racusin, J. L., Liang, E. W., Burrows, D. N., et al. 2009, ApJ, 698, 43
- Racusin, J. L., Oates, S. R., Schady, P., et al. 2011, ApJ, 738, 138
- Rees, M. J., & Mészáros, P. 1998, ApJ, 496, L1

- Rhoads, J. E. 1999, ApJ, 525, 737
- Robertson, B. E., & Ellis, R. S. 2012, ApJ, 744, 95
- Rol, E., Jakobsson, P., Tanvir, N., & Levan, A. 2006, GRB Coordinates Network, 5555
- Sakamoto, T. 2005, GRB Coordinates Network, 3848
- Sakamoto, T., Lamb, D. Q., Kawai, N., et al. 2005a, ApJ, 629, 311
- Sakamoto, T., Ricker, G., Atteia, J.-L., et al. 2005b, GRB Coordinates Network, 3189
- Sakamoto, T., Barbier, L., Barthelmy, S. D., et al. 2006, ApJ, 636, L73
- Sakamoto, T., Barthelmy, S. D., Evans, P. A., et al. 2008, GRB Coordinates Network, 8292
- Santana, R., Barniol Duran, R., & Kumafr, P. 2014, ApJ, 785, 29
- Sari, R., & Mészáros, P. 2000, ApJ, 535, L33
- Sari, R., Piran, T., & Halpern, J. P. 1999, ApJ, 519, L17
- Sari, R., Piran, T., & Narayan, R. 1998, ApJ, 497, L17
- Sato, G., Yamazaki, R., Ioka, K., et al. 2007, ApJ, 657, 359
- Savaglio, S., Palazzi, E., Ferrero, P., & Klose, S. 2007, GRB Coordinates Network, 6166
- Schady, P., & Sbarufatti, B. 2006, GRB Coordinates Network, 5861
- Schlegel, D. J., Finkbeiner, D. P., & Davis, M. 1998, ApJ, 500, 525
- Schulze, S., Klose, S., Björnsson, G., et al. 2011, A&A, 526, A23
- Shao, L., & Dai, Z. G. 2007, ApJ, 660, 1319
- Shen, R., Kumar, P., & Robinson, E. L. 2006, MNRAS, 371, 1441
- Sheth, K., Frail, D. A., White, S., et al. 2003, ApJ, 595, L33
- Soderberg, A. M., Berger, E., Kasliwal, M., et al. 2006, ApJ, 650, 261
- Stamatikos, M., Barthelmy, S. D., Baumgartner, W., et al. 2008, GRB Coordinates Network, 8222
- Starling, R. L. C., Wijers, R. A. M. J., Hughes, M. A., et al. 2005, MNRAS, 360, 305

- Svensson, K. M., Levan, A. J., Tanvir, N. R., Fruchter, A. S., & Strolger, L.-G. 2010, MNRAS, 405, 57
- Tagliaferri, G., Goad, M., Chincarini, G., et al. 2005, Nature, 436, 985
- Tanvir, N. R., & Ball, J. 2012, GRB Coordinates Network, 13532
- Tanvir, N. R., Wiersema, K., Levan, A. J., et al. 2012, GRB Coordinates Network, Circular Service, No. 13441, #1 (2012), 13441
- Tanvir, N. R., Rol, E., Levan, A. J., et al. 2010, ApJ, 725, 625
- Tello, J. C., Sanchez-Ramirez, R., Gorosabel, J., et al. 2012, GRB Coordinates Network, Circular Service, No. 13118, #1 (2012), 13118
- Thoene, C. C., de Ugarte Postigo, A., Vreeswijk, P. M., Malesani, D., & Jakobsson, P. 2008a, GRB Coordinates Network, 8058
- Thoene, C. C., Jakobsson, P., Fynbo, J. P. U., et al. 2007, GRB Coordinates Network, 6499
- Thoene, C. C., Malesani, D., Vreeswijk, P. M., et al. 2008b, GRB Coordinates Network, 7602
- Thoene, C. C., Levan, A., Jakobsson, P., et al. 2006, GRB Coordinates Network, 5373
- Thone, C. C., Fynbo, J. P. U., Goldoni, P., et al. 2013, MNRAS, 428, 3590
- Uhm, Z. L., & Zhang, B. 2014, ApJ, 780, 82
- Uhm, Z. L., Zhang, B., Hascoët, R., et al. 2012, ApJ, 761, 147
- Ukwatta, T. N., Barthelmy, S. D., Baumgartner, W. H., et al. 2009, GRB Coordinates Network, 9337
- Urata, Y., Huang, K.-Y., Kuo, P.-H., et al. 2007, PASJ, 59, L29
- Urata, Y., Huang, K., Im, M., et al. 2009, ApJ, 706, L183
- Urata, Y., Huang, K., Takahashi, S., et al. 2014, ApJ, 789, 146
- van der Horst, A. J., Rol, E., Wijers, R. A. M. J., et al. 2005, ApJ, 634, 1166
- Vergani, S. D., Flores, H., Covino, S., et al. 2011, A&A, 535, A127
- von Kienlin, A. 2013, GRB Coordinates Network, Circular Service, No. 14473, #1 (2013), 14473

- Vreeswijk, P., Jakobsson, P., Ledoux, C., Thoene, C., & Fynbo, J. 2006, GRB Coordinates Network, 5535
- Vreeswijk, P., Malesani, D., Fynbo, J., et al. 2008a, GRB Coordinates Network, 8301
- Vreeswijk, P. M., Milvang-Jensen, B., Smette, A., et al. 2008b, GRB Coordinates Network, 7451
- Vreeswijk, P. M., Thoene, C. C., Malesani, D., et al. 2008c, GRB Coordinates Network, 7601
- Wang, F.-Y., Qi, S., & Dai, Z.-G. 2011, MNRAS, 415, 3423
- Wang, X.-G., Liang, E.-W., Li, L., et al. 2013, ApJ, 774, 132
- Wang, X.-G., Zhang, B., Liang, E.-W., et al. 2015, ApJS, 219, 9
- Wang, X.-Y., & Mészáros, P. 2006, ApJ, 643, L95
- Wei, D. M., & Lu, T. 2002, MNRAS, 332, 994
- Wei, J., Cordier, B., Antier, S., et al. 2016, ArXiv e-prints, arXiv:1610.06892
- Wiersema, K., Tanvir, N., Vreeswijk, P., et al. 2008, GRB Coordinates Network, 7517
- Willingale, R., O'Brien, P. T., Osborne, J. P., et al. 2007, ApJ, 662, 1093
- Woosley, S. E. 1993, ApJ, 405, 273
- Woosley, S. E., & Bloom, J. S. 2006, ARA&A, 44, 507
- Wu, X. F., Dai, Z. G., & Liang, E. W. 2004, ApJ, 615, 359
- Xin, L. P., Zheng, W. K., Wang, J., et al. 2010, MNRAS, 401, 2005
- Xu, D., de Ugarte Postigo, A., Malesani, D., et al. 2013, GRB Coordinates Network, Circular Service, No. 14757, #1 (2013), 14757
- Yonetoku, D., Yamazaki, R., Nakamura, T., & Murakami, T. 2005, MNRAS, 362, 1114
- Yost, S. A., Harrison, F. A., Sari, R., & Frail, D. A. 2003, ApJ, 597, 459
- Yost, S. A., Swan, H. F., Rykoff, E. S., et al. 2007, ApJ, 657, 925
- Yuan, F., Schady, P., Racusin, J. L., et al. 2010, ApJ, 711, 870
- Zafar, T., Watson, D., Fynbo, J. P. U., et al. 2011, A&A, 532, A143

- Zeh, A., Klose, S., & Kann, D. A. 2006, ApJ, 637, 889
- Zhang, B. 2006, Nature, 444, 1010
- . 2011, Comptes Rendus Physique, 12, 206
- Zhang, B., Fan, Y. Z., Dyks, J., et al. 2006, ApJ, 642, 354
- Zhang, B., & Mészáros, P. 2001, ApJ, 552, L35
- . 2004, International Journal of Modern Physics A, 19, 2385
- Zhang, B., & Yan, H. 2011, ApJ, 726, 90
- Zhang, B., Liang, E., Page, K. L., et al. 2007, ApJ, 655, 989
- Zhang, B., Zhang, B.-B., Virgili, F. J., et al. 2009, ApJ, 703, 1696
- Zhang, B.-B., van Eerten, H., Burrows, D. N., et al. 2015, ApJ, 806, 15
- Zhang, S. N., Feroci, M., Santangelo, A., et al. 2016, in Proc. SPIE, Vol. 9905, Space Telescopes and Instrumentation 2016: Ultraviolet to Gamma Ray, 99051Q
- Zhang, W., & MacFadyen, A. 2009, ApJ, 698, 1261
- Zheng, W., & Deng, J. 2010, Science China Physics, Mechanics, and Astronomy, 53, 265

Table 1. The temporal decay index α and spectral index β in different afterglow models.

| CMB | Spectral regime | $\beta(p)$ | $\alpha(\beta)/\alpha(\beta, q)$ | $\alpha(\beta)/\alpha(\beta, q)$ |
|---|-----------------------|-----------------|---|--|
| | | $p > 2$ | | $1 < p < 2$ |
| Pre-jet break phase without energy injection | | | | |
| ISM II | $\nu_m < \nu < \nu_c$ | $\frac{p-1}{2}$ | $\frac{3\beta}{2}$ | $\frac{6\beta+9}{16}$ |
| ISM I | $\nu > \nu_c$ | $\frac{p}{2}$ | $\frac{3\beta-1}{2}$ | $\frac{3\beta+5}{8}$ |
| Wind II | $\nu_m < \nu < \nu_c$ | $\frac{p-1}{2}$ | $\frac{3\beta+1}{2}$ | $\frac{2\beta+9}{8}$ |
| Wind I | $\nu > \nu_c$ | $\frac{p}{2}$ | $\frac{3\beta-1}{2}$ | $\frac{2\beta+6}{8}$ |
| Pre-jet break phase with energy injection | | | | |
| ISM II | $\nu_m < \nu < \nu_c$ | $\frac{p-1}{2}$ | $(q-1) + \frac{(2+q)\beta}{2}$ | $\frac{19q-10}{16} + \frac{(2+q)\beta}{8}$ |
| ISM I | $\nu > \nu_c$ | $\frac{p}{2}$ | $\frac{q-2}{2} + \frac{(2+q)\beta}{2}$ | $\frac{7q-2}{8} + \frac{(2+q)\beta}{8}$ |
| Wind II | $\nu_m < \nu < \nu_c$ | $\frac{p-1}{2}$ | $\frac{q}{2} + \frac{(2+q)\beta}{2}$ | $\frac{5q+4}{8} + \frac{\beta q}{4}$ |
| Wind I | $\nu > \nu_c$ | $\frac{p}{2}$ | $\frac{q-2}{2} + \frac{(2+q)\beta}{2}$ | $\frac{(\beta+3)q}{4}$ |
| Post-jet break phase without energy injection | | | | |
| ISM II | $\nu_m < \nu < \nu_c$ | $\frac{p-1}{2}$ | $\frac{6\beta+3}{4}$ | $\frac{3(2\beta+7)}{16}$ |
| ISM I | $\nu > \nu_c$ | $\frac{p}{2}$ | $\frac{6\beta+1}{4}$ | $\frac{3\beta+11}{8}$ |
| Wind II | $\nu_m < \nu < \nu_c$ | $\frac{p-1}{2}$ | $\frac{3\beta+2}{2}$ | $\frac{2\beta+13}{8}$ |
| Wind I | $\nu > \nu_c$ | $\frac{p}{2}$ | $\frac{3\beta}{2}$ | $\frac{\beta+5}{4}$ |
| Post-jet break phase with energy injection | | | | |
| ISM II | $\nu_m < \nu < \nu_c$ | $\frac{p-1}{2}$ | $\frac{5q-2}{4} + \frac{(2+q)\beta}{2}$ | $\frac{11q-2}{8} + \frac{(2+q)\beta}{8}$ |
| ISM I | $\nu > \nu_c$ | $\frac{p}{2}$ | $\frac{3q-2+2\beta(q+2)}{4}$ | $\frac{9q+2+\beta(q+2)}{8}$ |
| Wind II | $\nu_m < \nu < \nu_c$ | $\frac{p-1}{2}$ | $\frac{q}{2} + \frac{(2+q)\beta}{2}$ | $\frac{1}{2} + \frac{(2\beta+9)q}{8}$ |
| Wind I | $\nu > \nu_c$ | $\frac{p}{2}$ | $\frac{\beta(q+2)-2(1-q)}{2}$ | $\frac{(\beta+5)q}{4}$ |

Table 2—Continued

| GRB | β_O | α_1 | α_2 | t_b^a | z | Ref. for β_O and z^b | E_p^c | INST ^d | INST and Ref. for E_p^e |
|---------|-----------------|------------------|-----------------|-------------------|--------|------------------------------|---------------|-------------------|---------------------------|
| 090926A | 0.72 ± 0.17 | 1.20 ± 0.13 | 2.50 ± 0.21 | 1024.1 ± 42.2 | 2.1062 | (8);(49) | 321 ± 12 | FER/KON/SWI/SUZ | FER,(79) |
| 091029 | 0.57 | 0.54 ± 0.11 | 1.47 ± 0.09 | 30.0 ± 6.8 | 2.752 | (4);(50) | 36 ± 2 | SWI | |
| 091127 | 0.43 ± 0.1 | 0.69 ± 0.00 | 1.47 ± 0.12 | 55.0 ± 1.3 | 0.49 | (51);(52) | 61 ± 18 | SWI/FER | FER,(79) |
| 100219A | 0.60 ± 0.12 | 0.84 ± 0.08 | 1.75 ± 0.12 | 1.8 ± 0.4 | 4.80 | (53);(54) | | SWI | |
| 100219A | 0.66 ± 0.13 | -2.40 ± 0.17 | 1.70 ± 0.14 | 17.5 ± 5.4 | 4.80 | (53);(54) | | SWI | |
| 110205A | 1.12 ± 0.24 | 1.45 ± 0.12 | 2.31 ± 0.22 | 103.2 ± 8.0 | 2.22 | (55);(56) | 222 ± 74 | KON/SWI/SUZ | KON,(80) |
| 120729A | 1 ± 0.1 | 0.91 ± 0.12 | 2.14 ± 0.19 | 5.6 ± 0.5 | 0.8 | (57);(58) | 311 ± 20 | FER/SWI | FER,(81) |
| 130427A | 0.69 ± 0.01 | 1.01 ± 0.09 | 1.88 ± 0.11 | 127.9 ± 1.4 | 0.34 | (59);(60) | 933 ± 112 | KON/FER/SWI/RHE | FER,(82) |
| 130603B | -0.84 ± 0.1 | 1.11 ± 0.11 | 2.10 ± 0.21 | 31.0 ± 7.7 | 0.3564 | (61);(62) | 660 ± 100 | SWI/KON | KON,(83) |

^aBreak time, in unit of ks;

^bReferences for β_O and z ;

^cSpectral peak energy on observe-frame,, in unit of keV;

^dThe instrument name of the experiment(s), or of the satellite(s), that provided the estimates of spectral parameters and energy, CGO=*CGRO-BATSE*, FER=*Fermi-GBM*, HET=*HETE-2-FREGATE*, INT=*INTEGRAL-SPI/IBIS*, KON=*Konus-Wind*, RHE=*RHESSI*, SAX=*BeppoSAX*, SWI=*Swift-BAT*, SUZ=*Suzaku-WAM*;

^eReferences for E_p :(1)Liang & Zhang (2006); (2)Panaitescu (2005b);(3)Svensson et al. (2010);(4)Li et al. (2012);(5)Kann et al. (2010b); (6)Vreeswijk et al. (2006);(7)Kann et al. (2006);(8)Kann et al. (2010a) (9)Urata et al. (2007);(10)Mannucci et al. (2011);(11)de Pasquale et al. (2007);(12)Robertson & Ellis (2012); (13)Price et al. (2006);(14)Yost et al. (2007); (15)Guidorzi et al. (2007); (16)Soderberg et al. (2006);(17)Butler et al. (2007)(18)Fynbo et al. (2009); (19)Prochaska et al. (2007);(20)Ferrero et al. (2009); (21)Savaglio et al. (2007);(22)Zafar et al. (2011);(23)Thoene et al. (2006);(24)Perley et al. (2008d);(25)Schady & Sbarufatti (2006); (26)Wang et al. (2015);(27)Jakobsson et al. (2007b);(28)Xin et al. (2010);(29)Cenko et al. (2007); (30)Krühler et al. (2009a);(31)Perley et al. (2008c); (32)Prochaska et al. (2008);(33)D'Elia et al. (2009);(34)Vreeswijk et al. (2008b); (35)Thoene et al. (2008b);(36)Robertson & Ellis (2012);(37)Vreeswijk et al. (2008c); (38)Guidorzi et al. (2011);(39)Perley et al. (2008a);(40)Kann et al. (2011); (41)Perley et al. (2008b);(42)Yuan et al. (2010);(43)D'Avanzo et al. (2008);(44)Evans et al. (2009);(45)Landsman et al. (2008); (46)Nicuesa Guelbenzu et al. (2011b);(147)Levesque et al. (2009);(48)Cenko et al. (2009b);(49)Malesani et al. (2009); (50)Chornock et al. (2009b);(51)Vergani et al. (2011);(52)Cucchiara et al. (2009); (53)Thoene et al. (2013);(54)Groot et al. (2010);(55)Cucchiara et al. (2011);(56)Cenko et al. (2011); (57)Cano et al. (2014a);(58)Tanvir & Ball (2012);(59)Perley et al. (2014);(60)Levan et al. (2013); (61)Fong et al. (2014);(62)Xu et al. (2013);(63)Amati et al. (2008); (64)Jimenez et al. (2001);(65)Liang & Zhang (2005);(66)Price et al. (2003);(67)Sakamoto (2005);(68)Nava et al. (2012);(69)Cenko et al. (2006);(70)Sakamoto et al. (2008);(71)Golenetskii et al. (2006b); (72)Perley et al. (2008d);(73)Butler et al. (2010);(74)Golenetskii et al. (2008a);(75)Ohno et al. (2008);(76)Krimm et al. (2009);(77)Golenetskii et al. (2008c);(78)Kann et al. (2010b);(79)Guetta et al. (2011a);(80)Golenetskii et al. (2011);(81)Cano et al. (2014b); (82)von Kienlin (2013);(83)Golenetskii et al. (2013);

Table 3. Temporal and Spectral Parameters of GRBs with a Lower Limit of Jet Break Time.

| GRB | β_O | α | z | Ref. for β_O and z^a | E_p | INST | INST and Ref. for E_p ^a |
|---------|-------------|-------------|---------|------------------------------|------------|-----------------|--------------------------------------|
| 020124 | 0.91 ± 0.11 | 1.85 ± 0.11 | 3.2 | (1),(2) | 87 ± 15 | HET/KON | HET/KON,(44),(45) |
| 020813 | 0.85 ± 0.1 | 1.26 ± 0.24 | 1.25 | (1),(3) | 142 ± 13 | HET/KON | HET/KON,(44),(45) |
| 050401 | 0.5 ± 0.2 | 0.89 ± 0.08 | 2.899 | (4),(5) | 132 ± 16 | SWI/KON | KON,(46),(47) |
| 050416A | 0.92 ± 0.3 | 1.31 ± 0.09 | 0.6852 | (4),(6) | 15 ± 5 | SWI | SWI,(45),(47) |
| 050603 | 0.71 ± 0.1 | 1.7 ± 0.13 | 2.821 | (4),(7) | 349 ± 28 | SWI/KON/INT | KON,(47),(48) |
| 050721 | 1.16 ± 0.35 | 1.09 ± 0.11 | (8),(-) | | | SWI | |
| 051028 | 0.6 ± 0 | 0.99 ± 0.1 | 3.7 | (4),(9) | 298 ± 73 | HET/KON | KON,(49) |
| 060210 | 0.37 ± 0.08 | 1.31 ± 0.11 | 3.9133 | (4),(9) | | SWI | |
| 060512 | 0.24 ± 0.2 | 1.11 ± 0.09 | 1.8836 | (4),(10) | 124 ± 38 | SWI/SUZ | |
| 060714 | 1.02 ± 0.05 | 1.62 ± 0.08 | 1.2622 | (4),(11) | 399 ± 19 | RHE/SUZ/KON/SWI | |
| 060904B | 1.11 ± 0.1 | 1.01 ± 0.21 | 0.7029 | (4),(12) | | SWI | |
| 060906 | 0.56 ± 0.02 | 1.02 ± 0.15 | 3.6856 | (4),(13) | | SWI | |
| 060908 | 0.98 ± 0.42 | 1.12 ± 0.13 | 1.949 | (4),(14) | 307 ± 92 | SWI/KON | KON,(50),(8) |
| 060912A | 0.6 ± 0.15 | 0.94 ± 0.01 | 0.937 | (4),(15) | | SWI/KON | |
| 060927 | 0.61 ± 0.05 | 1.3 ± 0.15 | 5.467 | (4),(16) | | SWI | |
| 061007 | 0.68 ± 0.02 | 1.31 ± 0.05 | 2.602 | (4),(11) | 485 ± 67 | SWI/KON | KON,(51) |
| 070110 | 0.55 ± 0.04 | 1.2 ± 0.15 | 2.3521 | (4),(17) | | SWI | |
| 070306 | 0.43 ± 0 | 0.87 ± 0.01 | 2.2 | (4),(18) | | SWI | |
| 070311 | 1 ± 0.2 | 0.73 ± 0.21 | (4),(-) | | | INT | |
| 070318 | 0.78 ± 0.1 | 1.02 ± 0.09 | 0.84 | (4),(17) | | SWI | |
| 070611 | 0.73 ± 0 | 0.58 ± 0.12 | 2.0394 | (4),(19) | | SWI | |
| 071025 | 0.96 ± 0.14 | 1.28 ± 0.12 | 4.8 | (8),(20) | | SWI | |
| 071031 | 0.74 ± 0.22 | 1.16 ± 0.09 | 2.692 | (4),(4) | 451 ± 73 | SWI/KON | |
| 071112C | 0.63 ± 0.29 | 0.94 ± 0.15 | 0.8227 | (4),(21) | | SWI | |
| 080319A | 0.77 ± 0.02 | 0.65 ± 0.11 | 2.2 | (4),(22) | 654 ± 14 | SWI/INT | |
| 080319C | 0.85 ± 0.05 | 0.94 ± 0.05 | 1.95 | (4),(23) | 4400 ± 400 | SWI/KON/SUZ/FER | KON,(52) |
| 080721 | 0.36 ± 0 | 1.27 ± 0.05 | 2.591 | (8),(24) | | SWI | |
| 080804 | 0.7 ± 0.4 | 1.07 ± 0.08 | 2.2045 | (8),(25) | 56 ± 6 | SWI/FER | |
| 080913 | 0.79 ± 0.03 | 0.98 ± 0.11 | 6.7 | (4),(26) | 121 ± 39 | SWI/KON/FER/INT | SWI/KON,(53) |
| 080928 | 1.32 ± 0.02 | 2.1 ± 0.22 | 1.692 | (4),(27) | | SWI | |
| 090102 | 0.74 ± 0.22 | 1.49 ± 0.12 | 1.547 | (4),(28) | 451 ± 73 | SWI/KON | KON,(54) |
| 090323 | 0.74 ± 0.15 | 1.55 ± 0.13 | 3.57 | (4),(29) | 416 ± 76 | KON/FER | KON,(55) |
| 090328 | 0.52 ± 0.02 | 0.96 ± 0.04 | 0.736 | (8),(30) | 1060 ± 60 | SWI/INT/FER/KON | FER,(56),(8) |
| 090510 | 0.68 ± 0.05 | 0.81 ± 0.05 | 0.4428 | (31),(32) | | SWI | |
| 090812 | 0.44 ± 0.04 | 1.11 ± 0.15 | 2.452 | (4),(33) | | SWI | |
| 100418A | 0.7 ± 0.1 | 1.22 ± 0.11 | 0.624 | (34),(35) | | SWI | |
| 101024A | 0.64 ± 0.05 | 0.79 ± 0.05 | 2.69 | (36),(4) | | SWI | |
| 110918A | 0.63 ± 0.29 | 0.95 ± 0.11 | 0.982 | (37),(38) | | SWI | |
| 120326A | 0.75 ± 0.08 | 1.65 ± 0.14 | 1.798 | (39),(40) | 46 ± 4 | SWI/FER/SUZ | FER,(57) |
| 120711A | 0.98 ± 0.09 | 1.37 ± 0.13 | 1.405 | (41),(42) | | SWI | |
| 120815A | 0.78 ± 0.01 | 0.63 ± 0.12 | 2.358 | (4),(43) | | SWI | |

^aReferences for E_p : (1)Liang & Zhang (2006);(2)Firmani et al. (2006);(3)Price et al. (2002);(4)Li et al. (2012);(5)Golenetskii et al. (2005a);(6)Mannucci et al. (2011);(7)Robertson & Ellis (2012);(8)Li et al. (2012);(9)Nava et al. (2008);(10)Bloom et al. (2006);(11)Jakobsson et al. (2006b);(12)Fugazza et al. (2006);(13)Vreeswijk et al. (2006);(14)Rol et al. (2006);(15)Jakobsson et al. (2006a);(16)Fynbo et al. (2006);(17)Jaunsen et al. (2007a);(18)Jaunsen et al. (2007b);(19)Thoene et al. (2007);(20)Kann et al. (2010a);(21)Jakobsson et al. (2007a);(22)Barthelmy et al. (2008);(23)Wiersema et al. (2008);(24)Jakobsson et al. (2008);(25)Thoene et al. (2008a);(26)Stamatikos et al. (2008);(27)Vreeswijk et al. (2008a);(28)de Ugarte Postigo et al. (2009b);(29)Chornock et al. (2009a);(30)Cenko et al. (2009a);(31)Nicueta Guelbenzu et al. (2012);(32)Ukwatta et al. (2009);(33)de Ugarte Postigo et al. (2009a);(34)Jia et al. (2012);(35)Cucchiara & Fox (2010);(36)Gendre et al. (2011);(37)Frederiks et al. (2013);(38)Levan et al. (2011);(39)Urata et al. (2014);(40)Tello et al. (2012);(41)Martin-Carrillo et al. (2014);(42)Tanvir et al. (2012);(43)Malesani et al. (2012);(44)Liang & Zhang (2005);(45)Sakamoto et al. (2005a);(46)Golenetskii et al. (2005c);(47)Amati (2006);(48)Golenetskii et al. (2005d);(49)Golenetskii et al. (2005b);(50)Krimm et al. (2009);(51)Golenetskii et al. (2006a);(52)Golenetskii et al. (2008b);(53)Pal'Shin et al. (2008);(54)Golenetskii et al. (2009a);(55)Golenetskii et al. (2009b);(56)Guetta et al. (2011b);(57)Collazzi (2012).

Table 4. Temporal and Spectral Parameters of GRBs with a Upper Limit of Jet Break Time.

| GRB | β_O | α | z | Ref. for β_O and z^a | E_p | INST | INST and Ref. for E_p ^a |
|---------|-----------------|--------------------|--------|------------------------------|--------------|--------------------|--------------------------------------|
| 070125 | 0.59 ± 0.10 | 1.82805 ± 0.07 | 1.5471 | (1);(2) | 367 ± 65 | KON/SUZ/INT SWI | KON,(8),(9) |
| 071010A | 0.61 ± 0.12 | 2.1 ± 0.23 | 0.985 | (3);(4) | | | |
| 100901A | 0.52 ± 0.10 | 1.51 ± 0.07 | 1.408 | (5);(6) | | SWI | |

^a(1)Li et al. (2012);(2)Fox et al. (2007);(3)Greiner et al. (2011);(4)Robertson & Ellis (2012);(5)Gorbovskoy et al. (2012);(6)Chornock et al. (2010),(8)(Golenetskii et al. 2007), (9)(Amati et al. 2008)

Table 8. Results of Our Linear Regression Analysis for the Luminosity Correlations.

| Relations | Expressions | r^c | p^d | δ^e |
|---|---|-------|-------------|------------|
| $E_{p,z}(E_{\gamma,\text{iso}})$ (<i>Amati</i>) | $\frac{E_{p,z}}{100\text{keV}} \simeq (0.63 \pm 0.31)(\frac{E_{\gamma,\text{iso}}}{10^{52}\text{erg}})^{(0.69 \pm 0.07)}$ | 0.81 | $< 10^{-4}$ | 0.33 |
| $E_{p,z}(E_{\gamma})$ (<i>Ghirlanda</i>) | $\frac{E_{p,z}}{100\text{keV}} \simeq (7.9 \pm 4.8)(\frac{E_{\gamma}}{10^{51}\text{erg}})^{(0.44 \pm 0.17)}$ | 0.43 | 0.005 | - |
| $E_{p,z}(E_{\gamma,\text{iso}}, t_{b,z})$ (<i>Liang-Zhang</i>) ^a | $\frac{E_{p,z}}{100\text{keV}} = (1.2 \pm 0.3)(\frac{E_{\gamma,\text{iso}}}{10^{52}\text{erg}})^{(0.56 \pm 0.07)}(\frac{t_{b,z}}{\text{day}})^{(0.67 \pm 0.08)}$ | 0.85 | $< 10^{-4}$ | 0.15 |
| $E_{p,z}(E_{\gamma,\text{iso}}, t_{b,z})$ (<i>Liang-Zhang</i>) ^b | $\frac{E_{p,z}}{100\text{keV}} = (1.3 \pm 0.4)(\frac{E_{\gamma,\text{iso}}}{10^{52}\text{erg}})^{(0.49 \pm 0.07)}(\frac{t_{b,z}}{\text{day}})^{(-0.08 \pm 0.05)}$ | 0.67 | $< 10^{-4}$ | 0.22 |

^arelations for the late time jet break sample;

^brelations for the entire sample,including the early and late time jet break sample;

^c r is the spearman correlation coefficient;

^d p is the change probability;

^e δ is the dispersion.

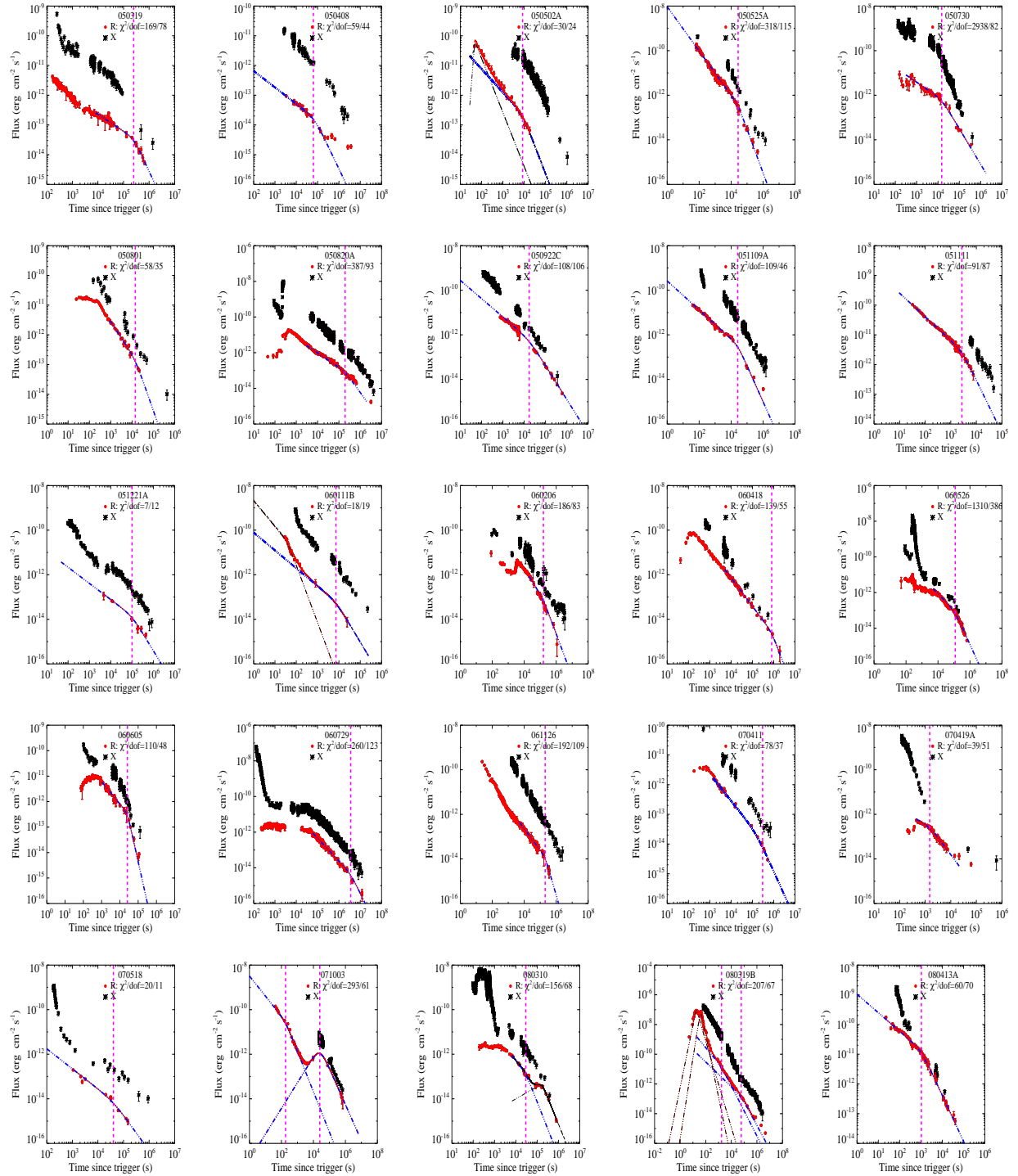


Fig. 1.— The observed light curves of the GRBs with one and more identified jet break(s). The optical lightcurves (red) are used to derive the jet break(s). The lightcurves are fit with the blue dotted-dashed lines, and the jet break times are shown by the purple vertical dashed lines. The X-ray lightcurves (black) are plotted for reference.

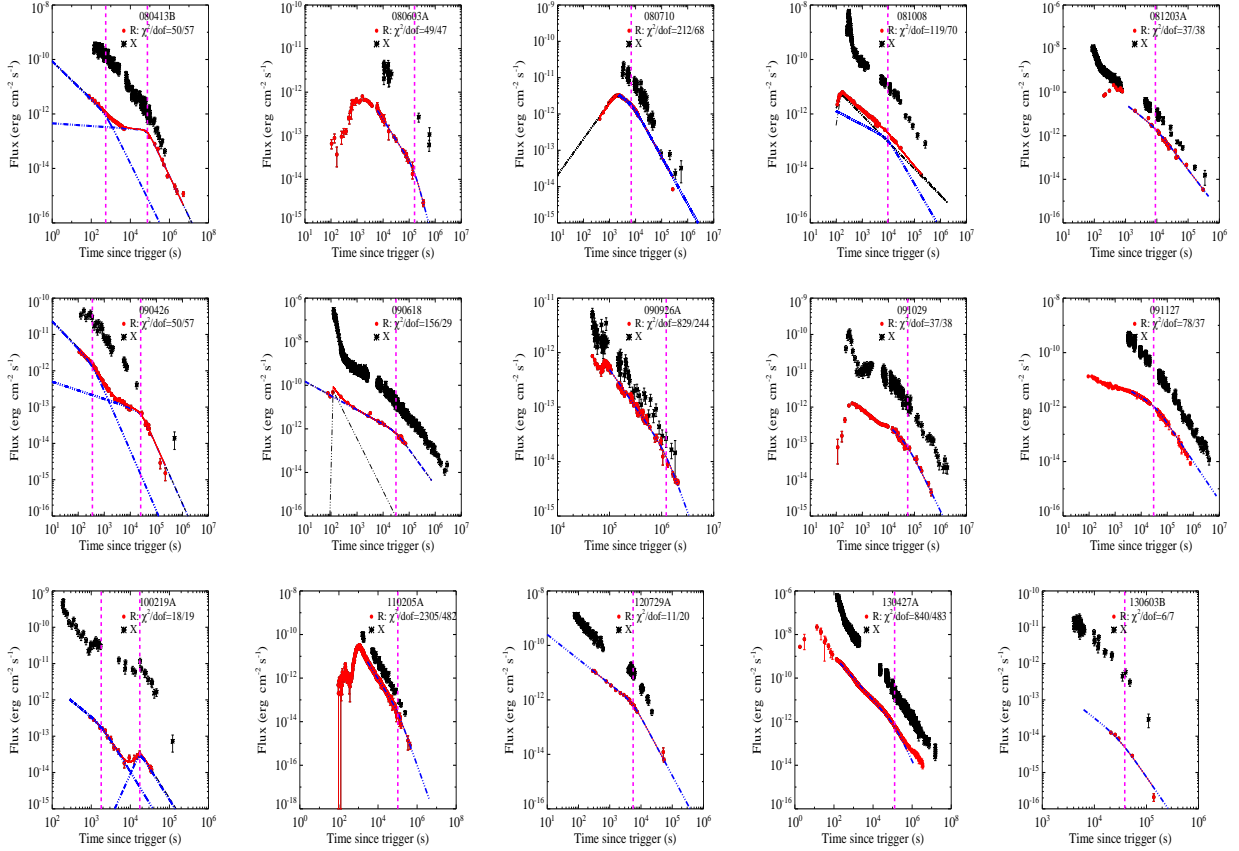


Figure. 1(Continued)

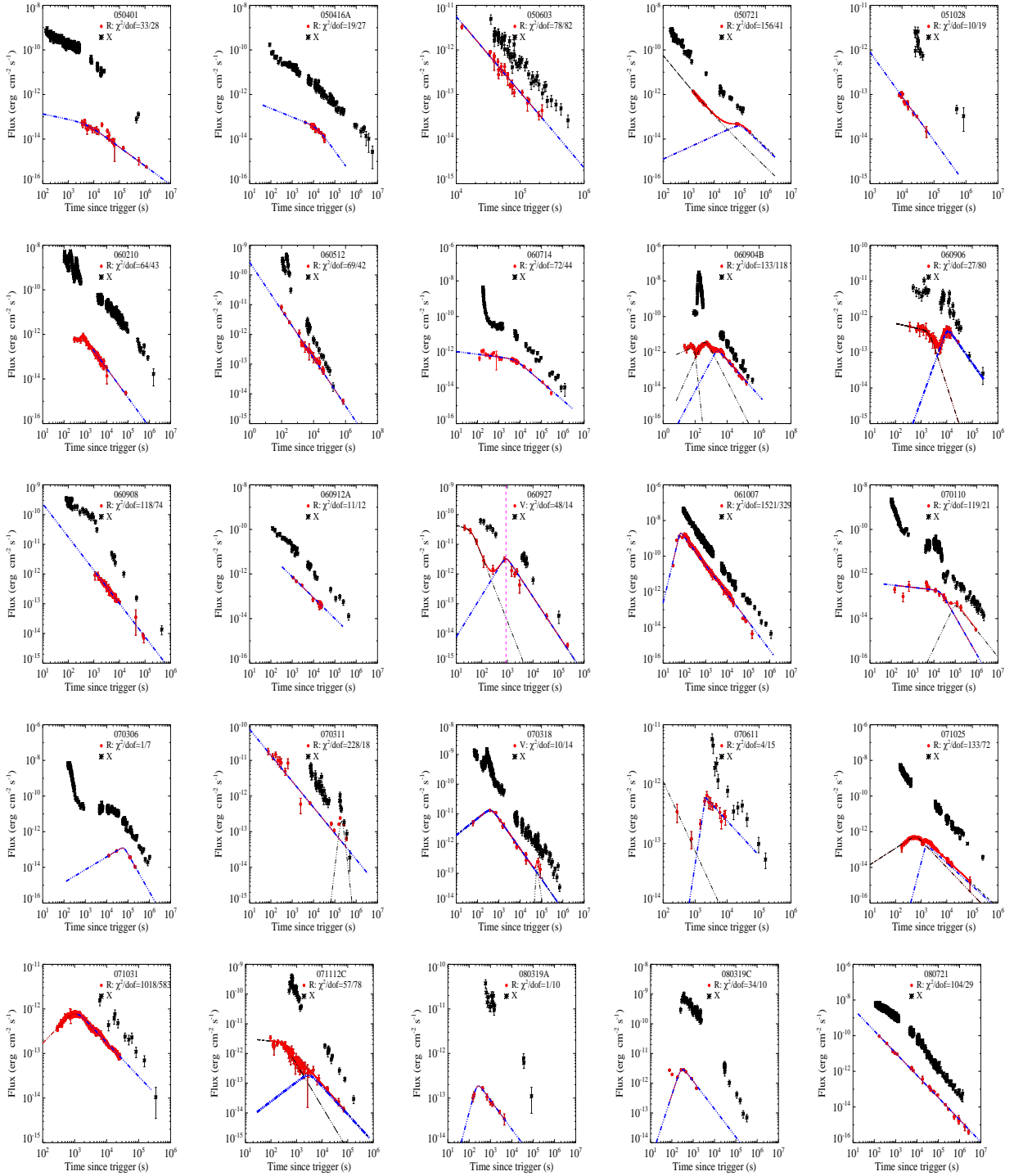


Fig. 2.— Same as Figure 1, but for the lower limit sample.

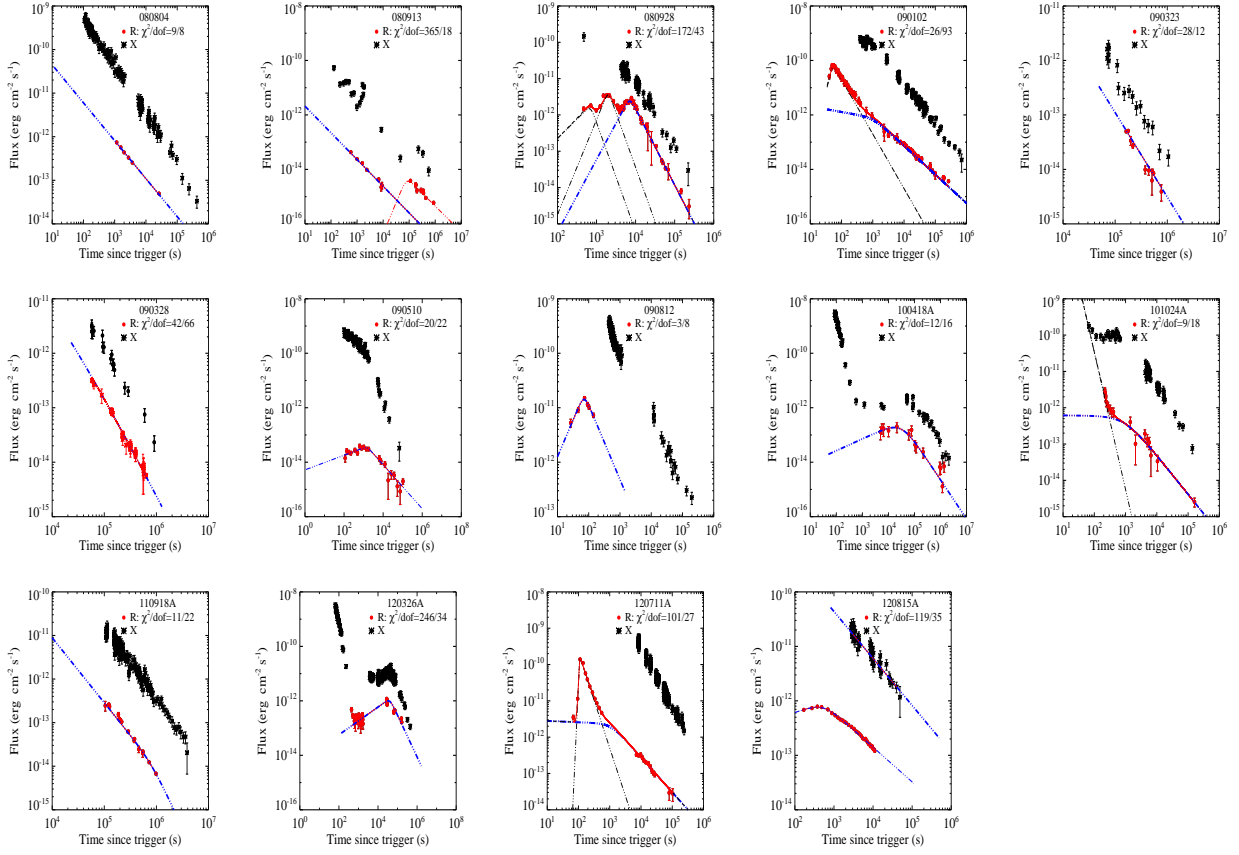


Figure. 2(Continued)

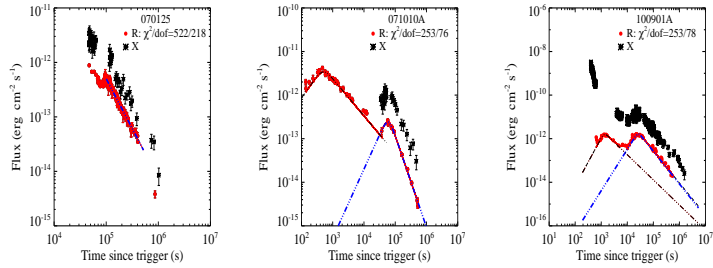


Fig. 3.— Same as Figure 1, but for the upper limit sample.

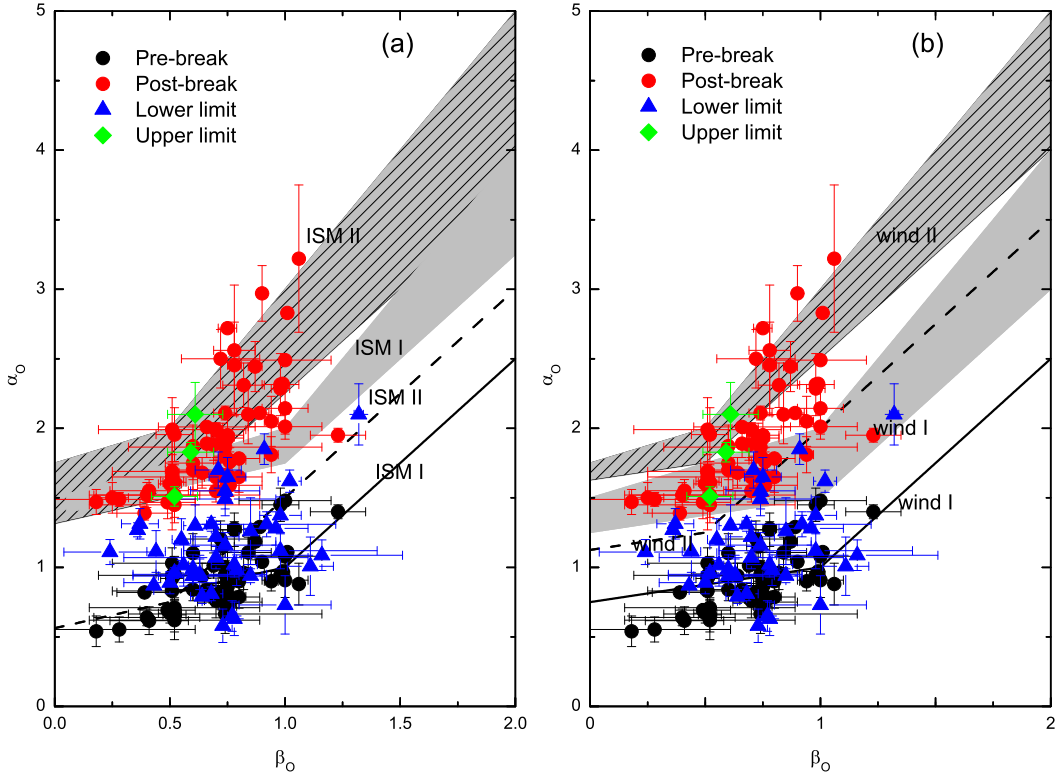


Fig. 4.— The measured afterglow α and β values compared against the closure relations of jet break in the external forward shock model. The thick solid lines and solid shaded regions indicate the closure relations for the pre-and post-break segments in spectral regime I ($\nu > \nu_c$). The lower and upper boundaries of the regions are defined with closure relation, respectively, without and with sideways expansion taken into account. Similarly, the thick dashed lines and hatched regions are for the emission in the spectral regime II ($\nu_m < \nu < \nu_c$). The black and red filled circles symbols represent the segments of pre- and post-break. The lower and upper limit sample marked as blue triangle and green diamond symbols, respectively. (a) ISM model; (b) wind model.

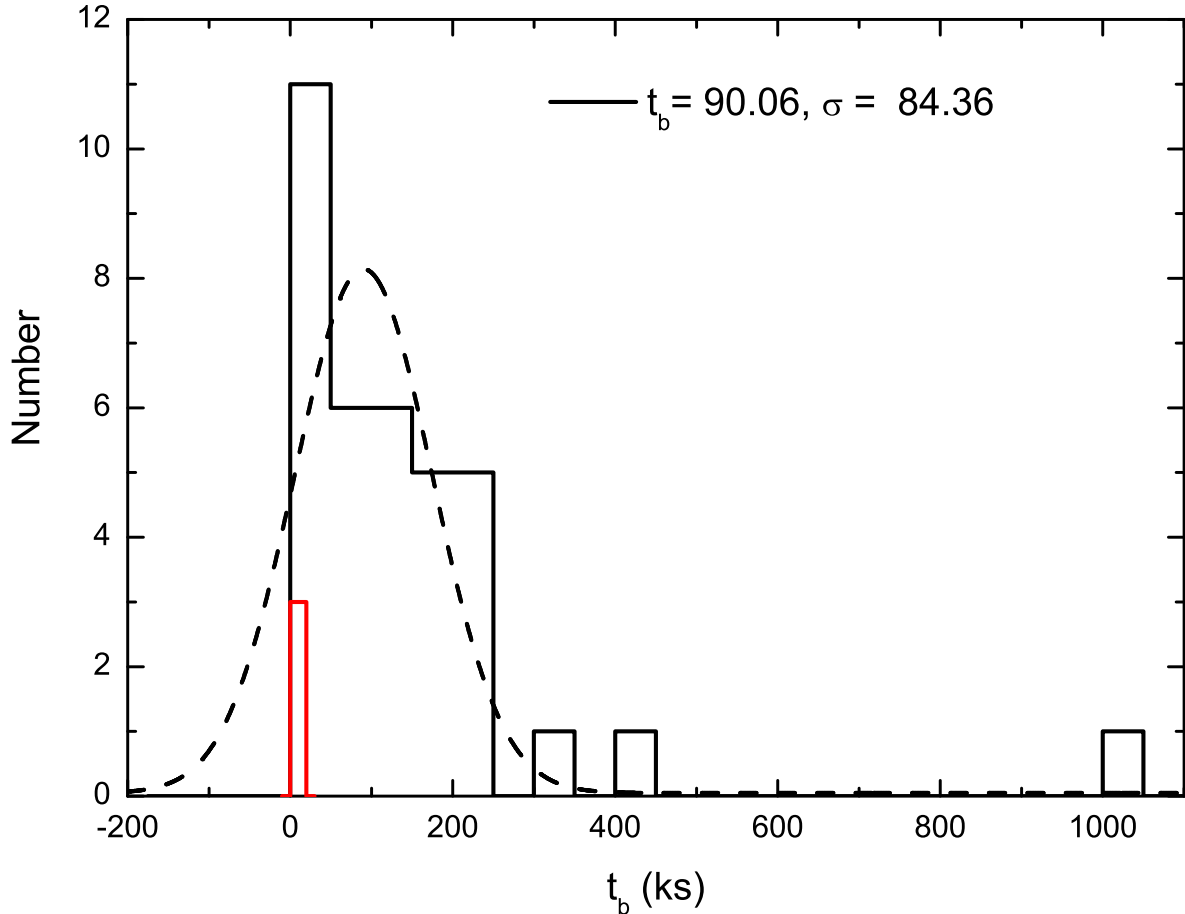


Fig. 5.— The distributions of the jet break time t_b (solid lines) and their best Gaussian fits (dash line). The typical values of the entire jet break sample (black) and the first jet of the two-component jet GRBs (red) **are** $t_b = 90.06 \pm 84.36$ ks **and** $t_b = 0.2 \sim 2$ ks, respectively.

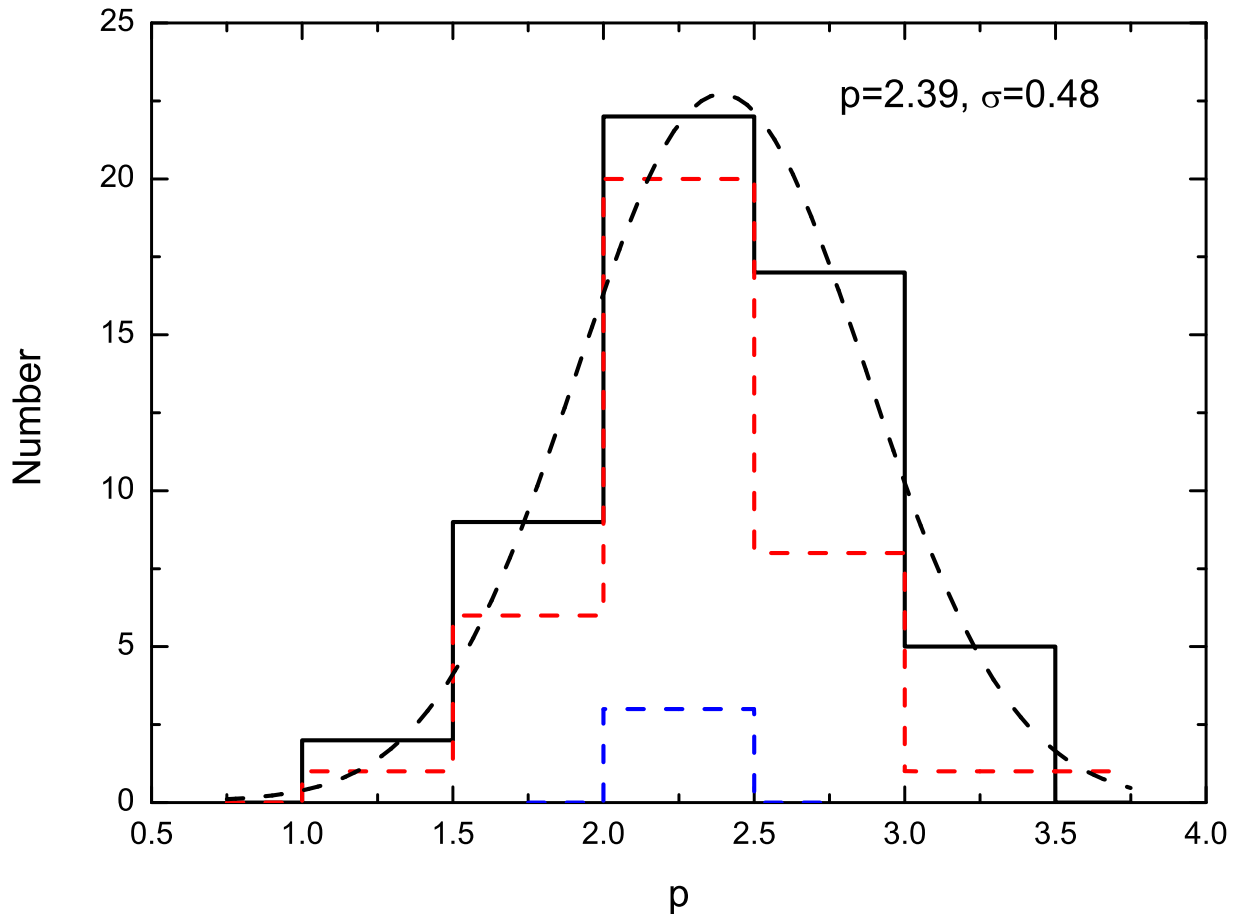


Fig. 6.— The distribution of the inferred electron spectral index p from jet break sample (black line), lower limit sample (red dashed line) and upper limit sample (blue dashed line). The black dashed line is the best Gaussian fit of the jet break sample, with $p = 2.39 \pm 0.48$.

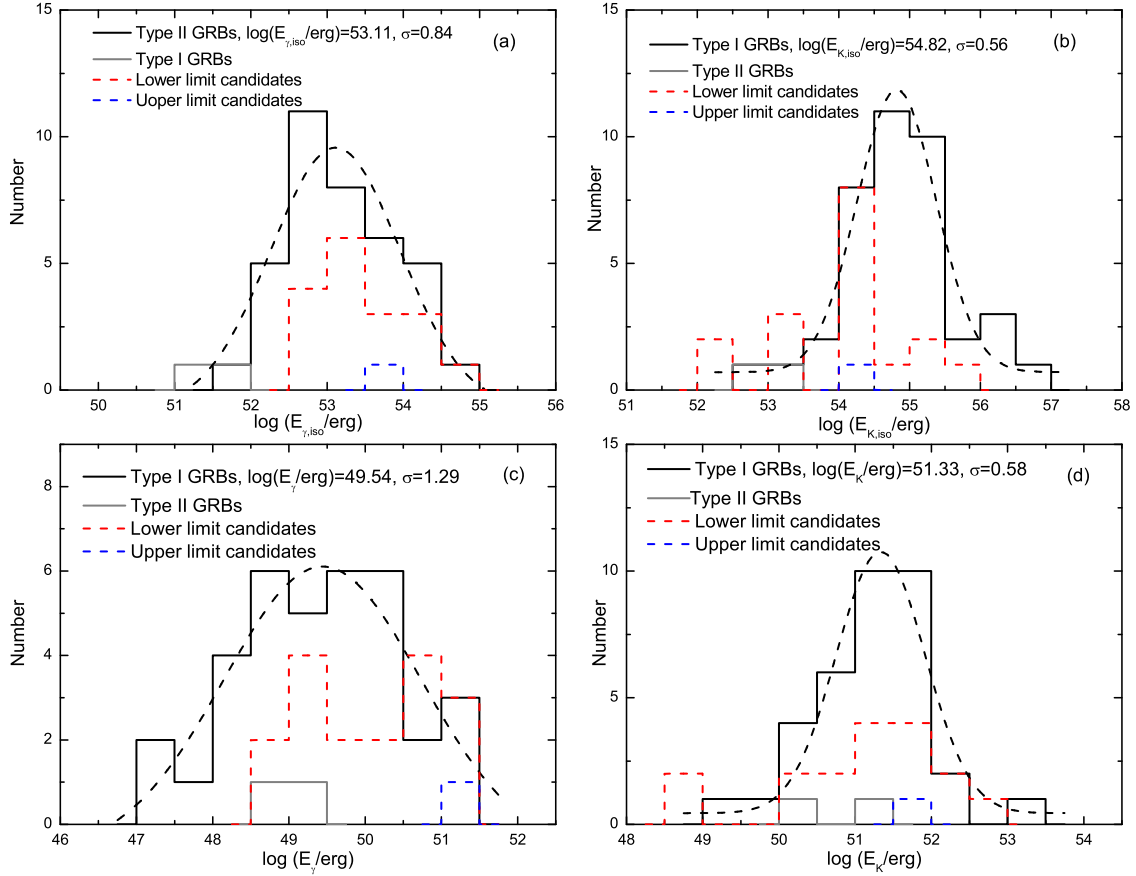


Fig. 7.— The distributions of γ -ray and kinetic energies derived from the jet break sample and the lower limit sample. The Type I and II GRBs in the jet break sample are denoted by gray and black line histograms, respectively. The lower and upper limit sample are represented as red and blue dashed line histogram. The black dashed lines are the best Gaussian fits for Type II GRBs: (a) isotropic γ -ray energy, $E_{\gamma,\text{iso}}$, with a typical value $\log(E_{\gamma,\text{iso}}/\text{erg}) = (53.11 \pm 0.84)$; (b) isotropic kinetic energy, with a typical value $\log(E_{K,\text{iso}}/\text{erg}) = (54.82 \pm 0.56)$; (c) geometrically corrected γ -ray energy (E_{γ}), with $\log(E_{\gamma}/\text{erg}) = (49.54 \pm 1.29)$; (d) geometrically corrected kinetic energy (E_K), with $\log(E_K/\text{erg}) = (51.33 \pm 0.58)$.

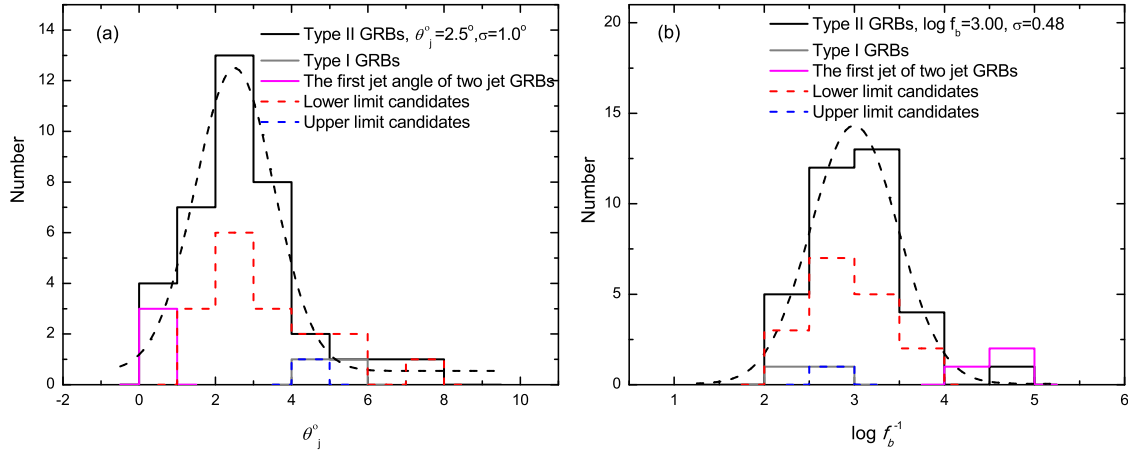


Fig. 8.— The distributions of (a)jet opening angle θ_j and (b) beaming factor f_b^{-1} . The Type I and II GRBs in the jet break sample are marked by gray and black line histograms, respectively. The lower and upper limit sample are represented as red and blue dashed line histogram. The opening angle and beaming factor of the first jet in the two jet breaks also marked with the magenta line. The black dashed lines are the best Gaussian fits of Type II GRBs, with $\theta_j = (2.5 \pm 1.0)^{\circ}$ and $\log f_b^{-1} = 3.00 \pm 0.48$.

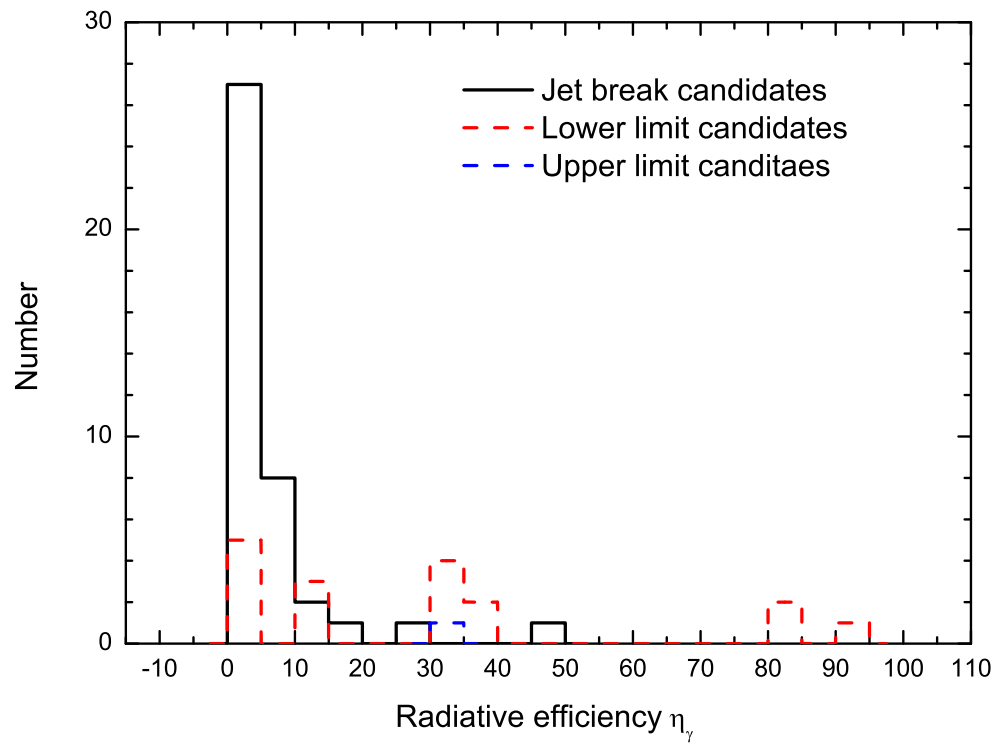


Fig. 9.— The distributions of radiative efficiency η_γ .

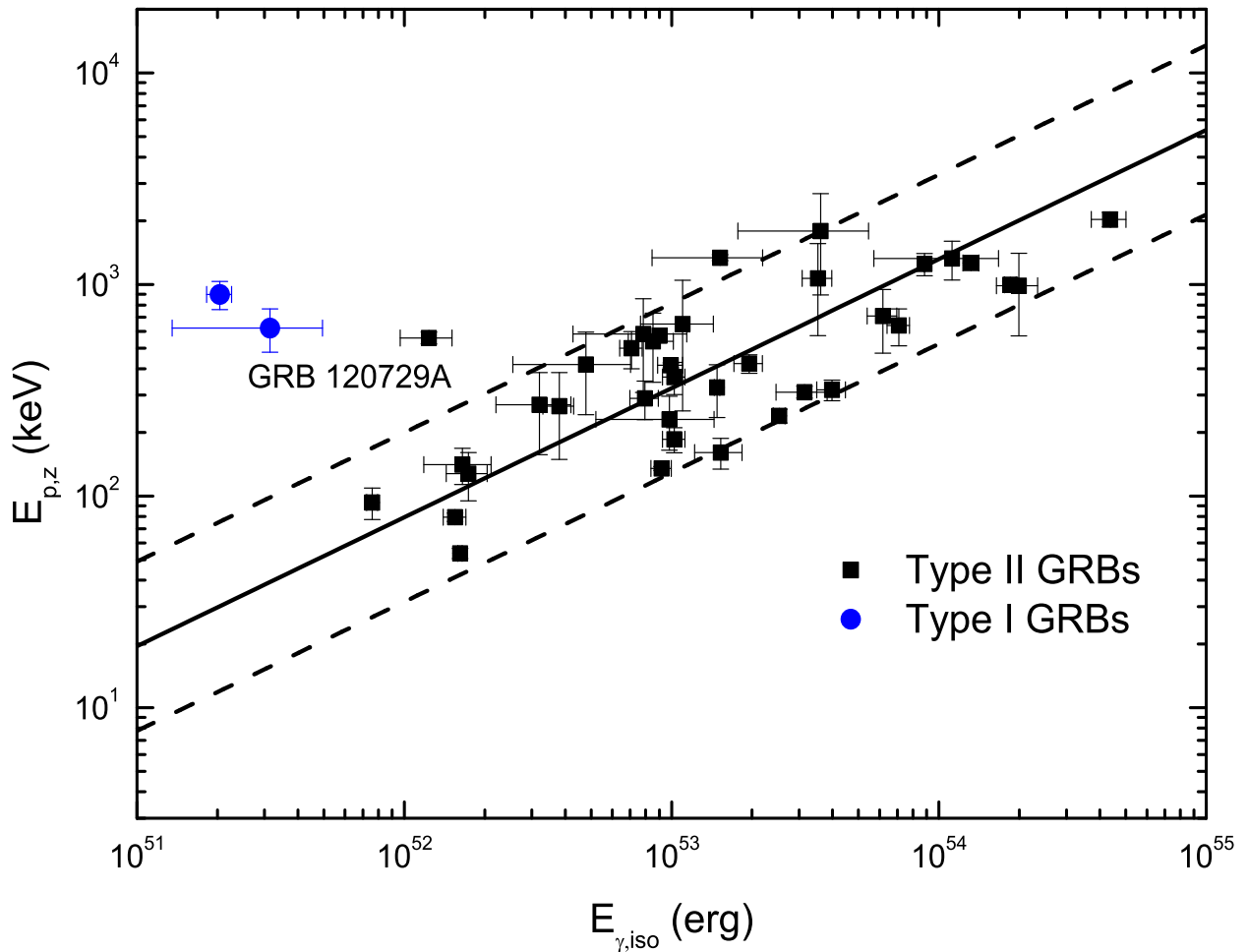


Fig. 10.— GRBs in $E_{\gamma,\text{iso}} - E_{\text{p},z}$ plane (*Amati* relation). The Type II and I GRBs are marked with black squares and blue circles, respectively. The solid line is the best fit with $\frac{E_{\text{p},z}}{100\text{keV}} \simeq (0.63 \pm 0.31) \left(\frac{E_{\gamma,\text{iso}}}{10^{52}\text{erg}} \right)^{(0.69 \pm 0.07)}$, and their 2σ dispersion regions are shown with the dashed lines.

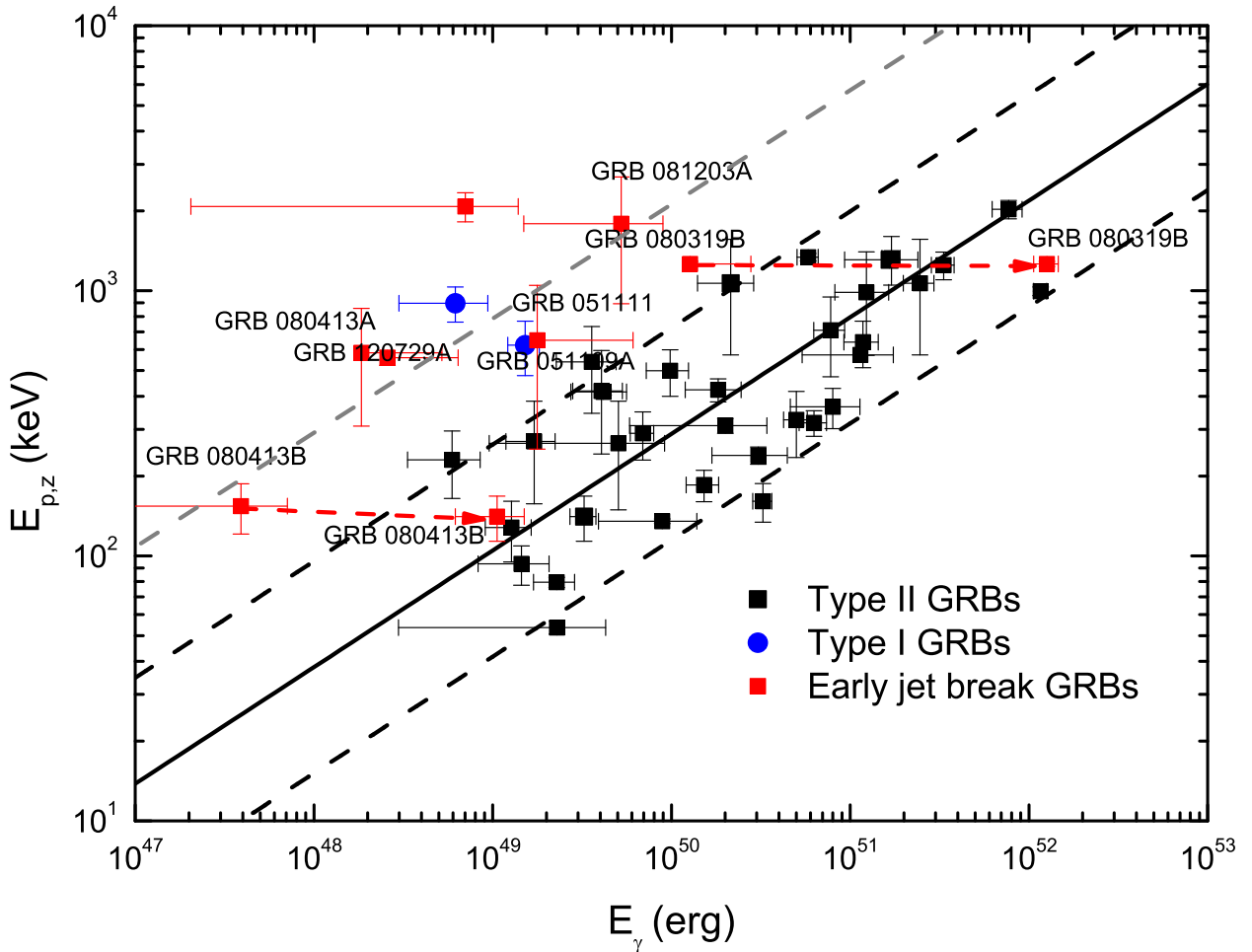


Fig. 11.— GRBs in $E_\gamma - E_{p,z}$ plane (Ghirlanda relation). The squares and circles symbols represent the Type II and I GRBs, respectively. The early jet breaks of Type II GRBs are marked with red squares. The red dashed lines with arrow are used to demonstrate the relation in two jet breaks from early one to the late one. The best fit line (solid) is $\frac{E_{p,z}}{100\text{keV}} \simeq (7.9 \pm 4.8)(\frac{E_\gamma}{10^{51}\text{erg}})^{(0.44 \pm 0.07)}$, and their 2σ dispersion regions are shown with the black dashed lines. The Type I GRBs and early jet break are located around a gray dashed line.

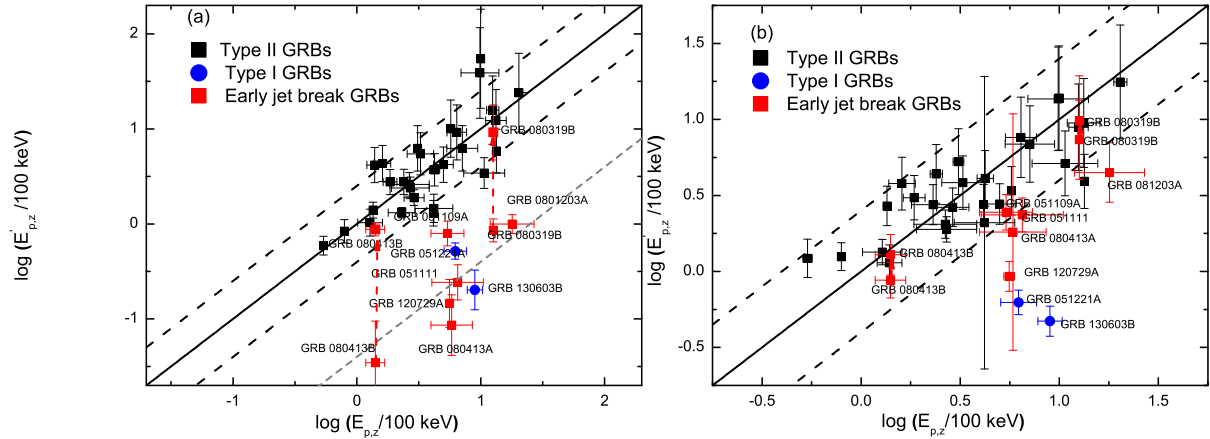


Fig. 12.— The comparisons of the $E_{p,z}$ and $E'_{p,z}$ calculated from the $E_{p,z} - E_{\gamma,\text{iso}} - t_{b,z}$ (*Liang-Zhang* relation) based on our sample. The squares and circles symbols represent the Type II and I GRBs, respectively. The early jet breaks of Type II GRBs are marked with red squares. The red dashed lines with arrow are used to demonstrate the relation in two jet breaks from early one to the late one. The best fit line (solid) and their 2σ dispersion regions (black dashed lines) are marked. (a) $\frac{E_{p,z}}{100\text{keV}} = (1.2 \pm 0.3)(\frac{E_{\gamma,\text{iso}}}{10^{52}\text{erg}})^{(0.56 \pm 0.07)}(\frac{t_{b,z}}{\text{day}})^{(0.67 \pm 0.08)}$ for the late jet break sample only. The Type I GRBs and early jet break are located around a gray dashed line. (b) $\frac{E_{p,z}}{100\text{keV}} = (1.3 \pm 0.4)(\frac{E_{\gamma,\text{iso}}}{10^{52}\text{erg}})^{(0.49 \pm 0.07)}(\frac{t_{b,z}}{\text{day}})^{(-0.08 \pm 0.05)}$ for all the Type II GRBs.

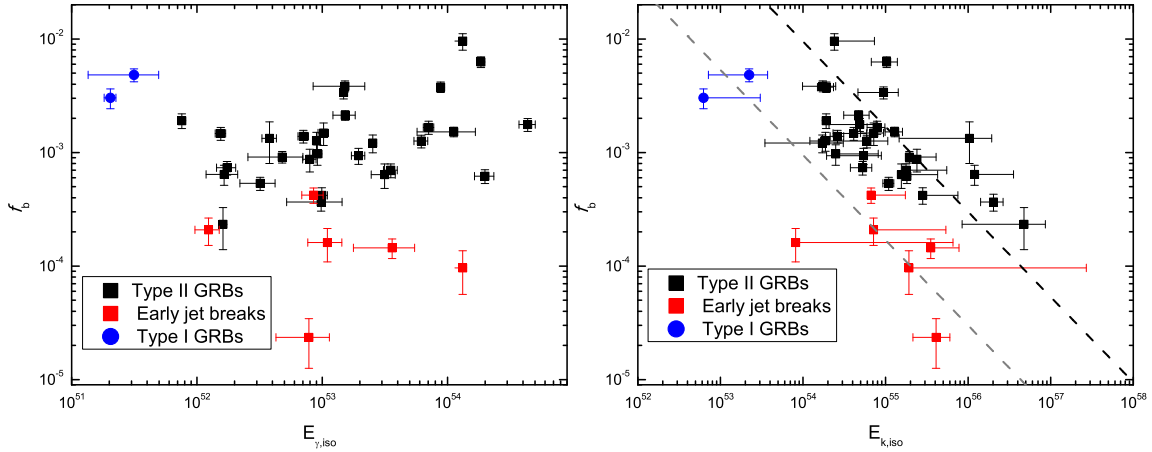


Fig. 13.— GRBs in the $E_{\gamma, \text{iso}}(E_{k, \text{iso}}) - f_b$ plane (*Frail* relation). The Type II and I GRBs are marked with black squares and blue circles, respectively. The early jet breaks of Type II GRBs are marked with red squares. (a) the comparisons of the $E_{\gamma, \text{iso}}$ and f_b . (b) the comparisons of the $E_{k, \text{iso}}$ and f_b , The Type II GRBs can be fitted with $E_{k, \text{iso}} \propto \sim f_b^{-0.8}$ (black dashed line). The Type I GRBs and early jet break are located around a gray dashed line.